Alexander N. Krot
Hawai‘i Institute of Geophysics & Planetology
University of Hawai‘i at Manoa, USA
sasha@higp.hawaii.edu

Lecture 1: Introduction to chondritic meteorites

Part I. Classification of chondritic meteorites

Part II. Chondritic components: Major characteristics & origin

Lecture 2: Chondrites & chondritic components: Implications for understanding processes in the solar nebula

Part I. Chronology of chondritic components

Part II. Origin & evolution of O-isotopic reservoirs in the early Solar System

UH Cosmochemistry group

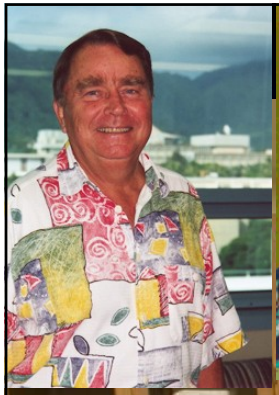

Meteorite classification

Chondrites

class →	Carbonaceous									Ordinary			Enstatite			
group →	CI	CM	CO	CR	CB		CH	CV	CK	H	L	LL	EH	EL	R	K
petr. type →	1	1-2	3-4	1-2	3		3	3-4	3-6	3-6			3-6		3-6	3
subgroup →					CB_a CB_b			CV_A CV_B CV_{red}								

Non-chondrites

Primitive

single asteroid?
- Acapulcoites
- Lodranites

single asteroid?
- Winonaites
- IAB silicate inclusions
- IIICD silicate inclusions

Differentiated

Achondrites

- Angrites
- Aubrites
- Brachinites
- Ureilites
- ***HED*** (*single asteroid (Vesta?)*)
  - Howardites
  - Eucrites
  - Diogenites
- ***Martian (SNC)*** (*Mars*)
  - Shergottites
  - Nakhlites
  - Chassignites
  - Orthopyroxenites
- *Moon*: Lunar

Stony-irons

- Mesosiderites
- Pallasites
  - main group
  - Eagle Station
  - pyroxene

Irons

IAB*
IC
IIAB
IIC
IID
IIE*
IIIAB
IIICD*
IIIE
IIIF
IVA*
IVB

- Based on chemical compositions & textures:
  - *chondritic meteorites* (escaped melting, but most experienced thermal processing on asteroids, such as aqueous alteration, thermal & shock metamorphism)
  - *non-chondritic meteorites*
    - *primitive achondrites* (experienced low degrees of melting & largely retained chondritic bulk chemical compositions)
    - *differentiated meteorites* (experienced partial or complete melting & differentiation)

Chondrites

- chondrites (exc. CI) consist of
  - chondrules
  - refractory inclusions
  - Fe,Ni-metal
  - fine-grained matrix
- chondrules, refractory inclusions & Fe,Ni-metal & most of matrix materials formed in the protoplanetary disk by high-temperature processes, such as evaporation, condensation & melting
- some portion of matrix materials escaped high-temperature processing

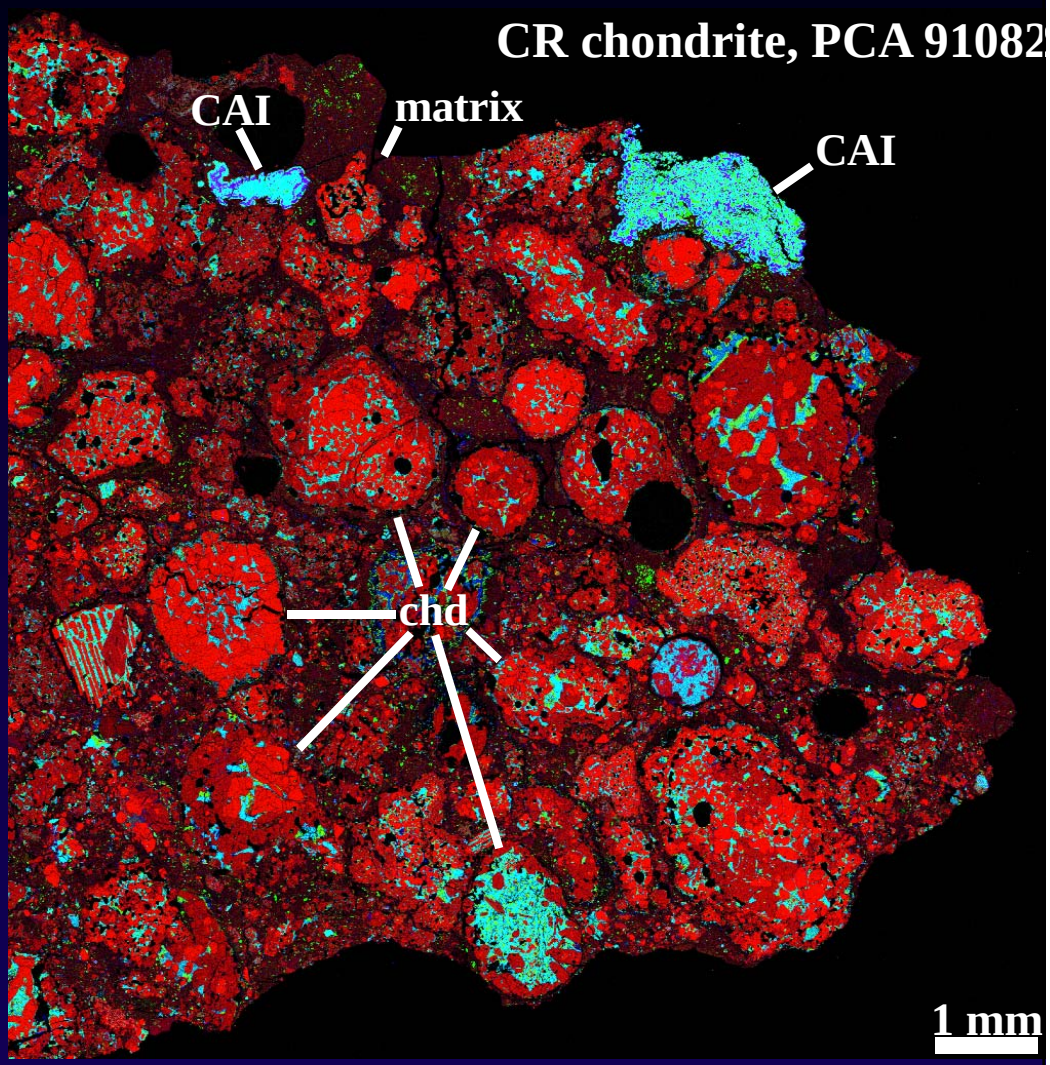

Classification of chondrites

- Based on bulk chemistry, O-isotopic compositions, mineralogy & petrography, chondrites are divided into 15 groups; 13 of them comprise three major *classes*

Carbonaceous
CI CM CO CV CK CR CH CB

Enstatite	*Ordinary*	Other
EH EL	H L LL	R K

- *Carbonaceous chondrites:* letters designating the groups refer to a typical member of a chondrite group (CI – *Ivuna-like*; CM – *Mighei-like*; CO – *Ornans-like*; CV – *Vigarano-like*; CK – *Karoonda-like*; CR – *Renazzo-like, CB – Bencubbin-like, CH – high metal*)
- *Enstatite chondrites:* EH & EL – high & low metallic iron
- *Ordinary chondrites:* letters designating the groups refer to bulk iron contents (H – high total iron; L – low total iron; LL – low metallic iron, low total iron)
- R – Rumuruti-like; K – Kakangari-like (grouplet composed of 2 members)
- *ungrouped* chondrites are chemically and/or mineralogically unique & cannot be classified into existing chondrite groups (e.g., Acfer 094, Adelaide)

CIs are compositionally most similar to the Sun

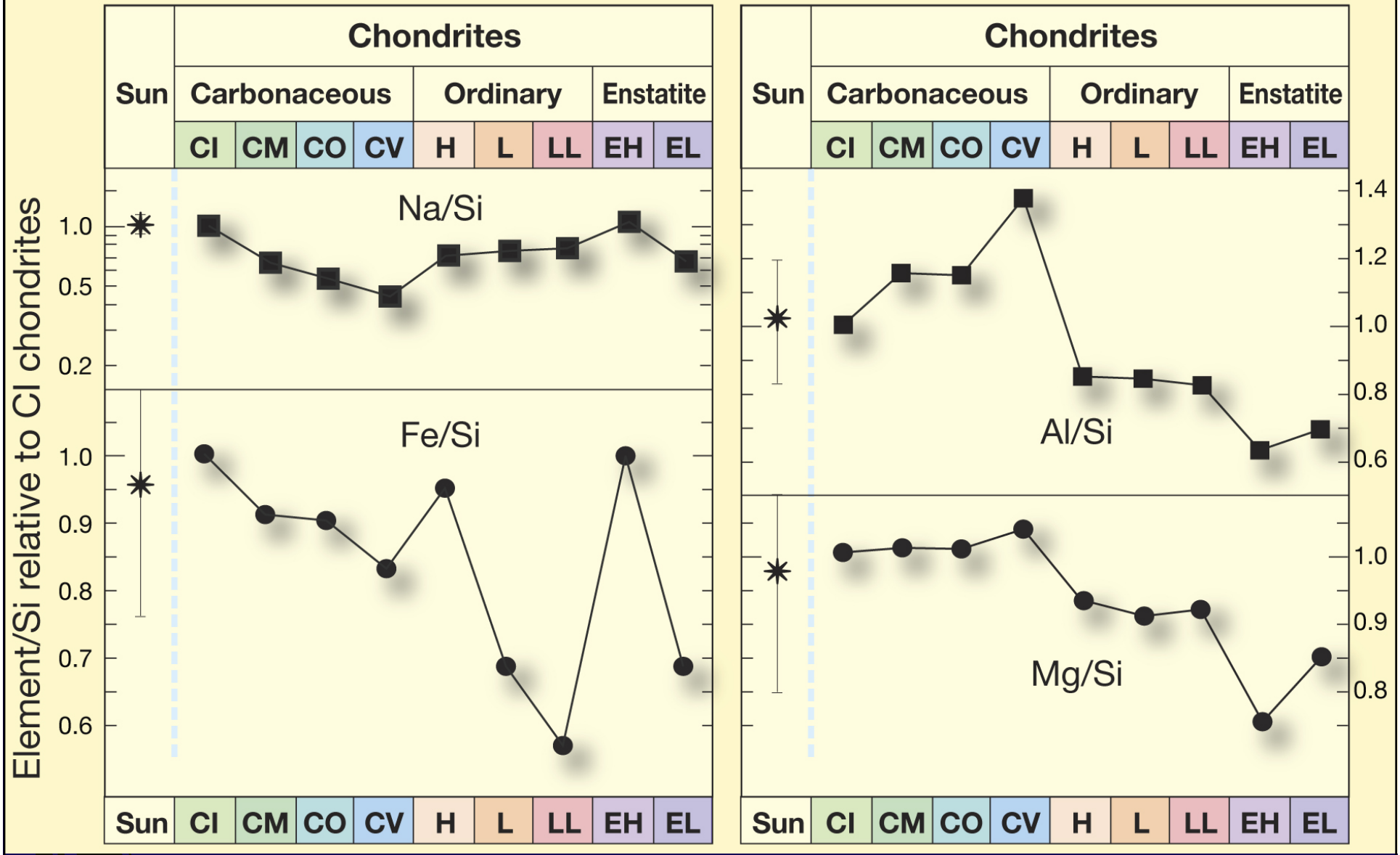

Palme & Jones (2003) TOG

Classification parameter: Bulk chemical composition

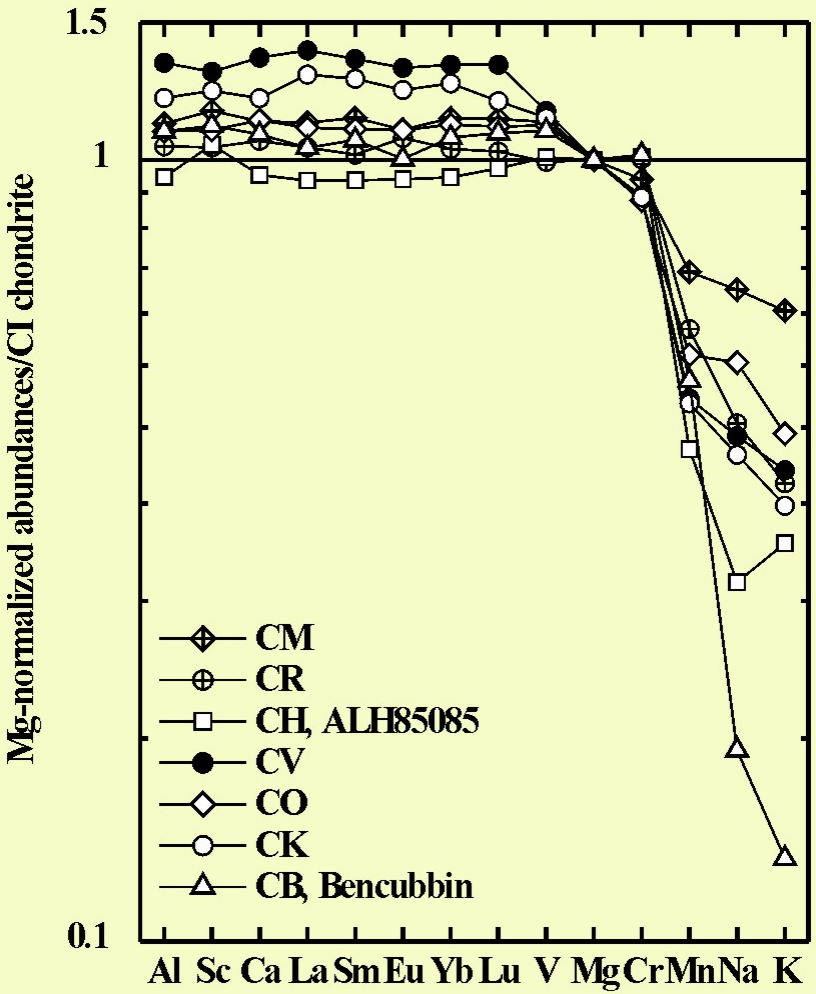

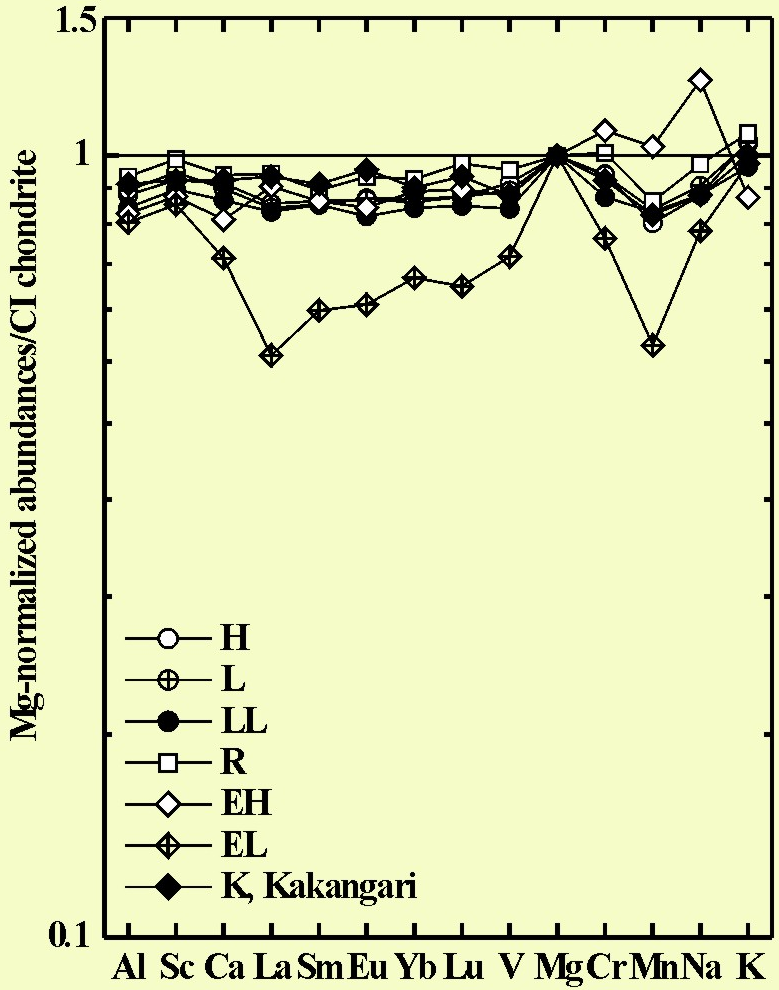

all data from Wasson & Kallemeyn

Classification parameter: Bulk chemical composition

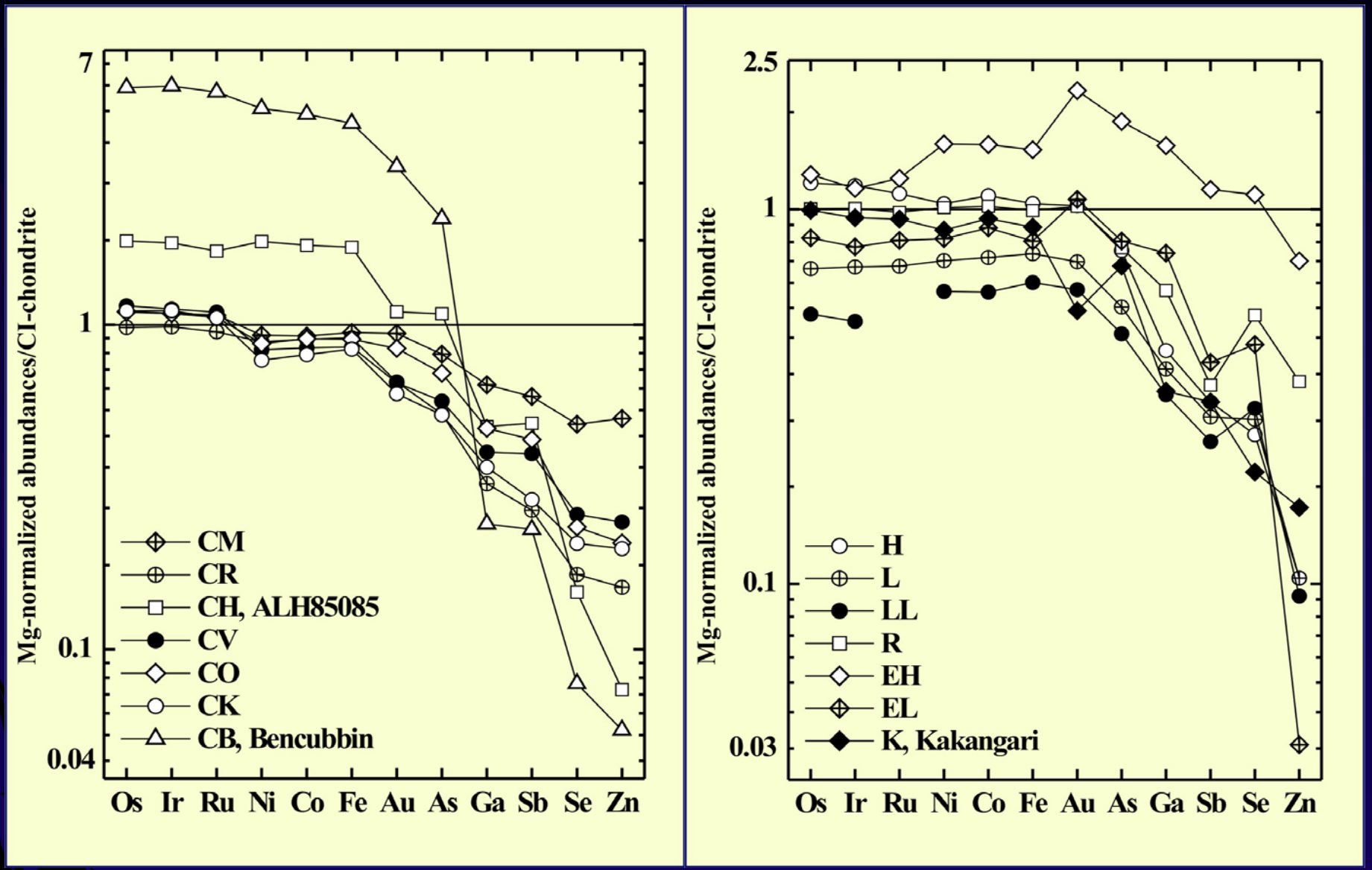

all data from Wasson & Kallemeyn

Classification parameter: O-isotopic composition

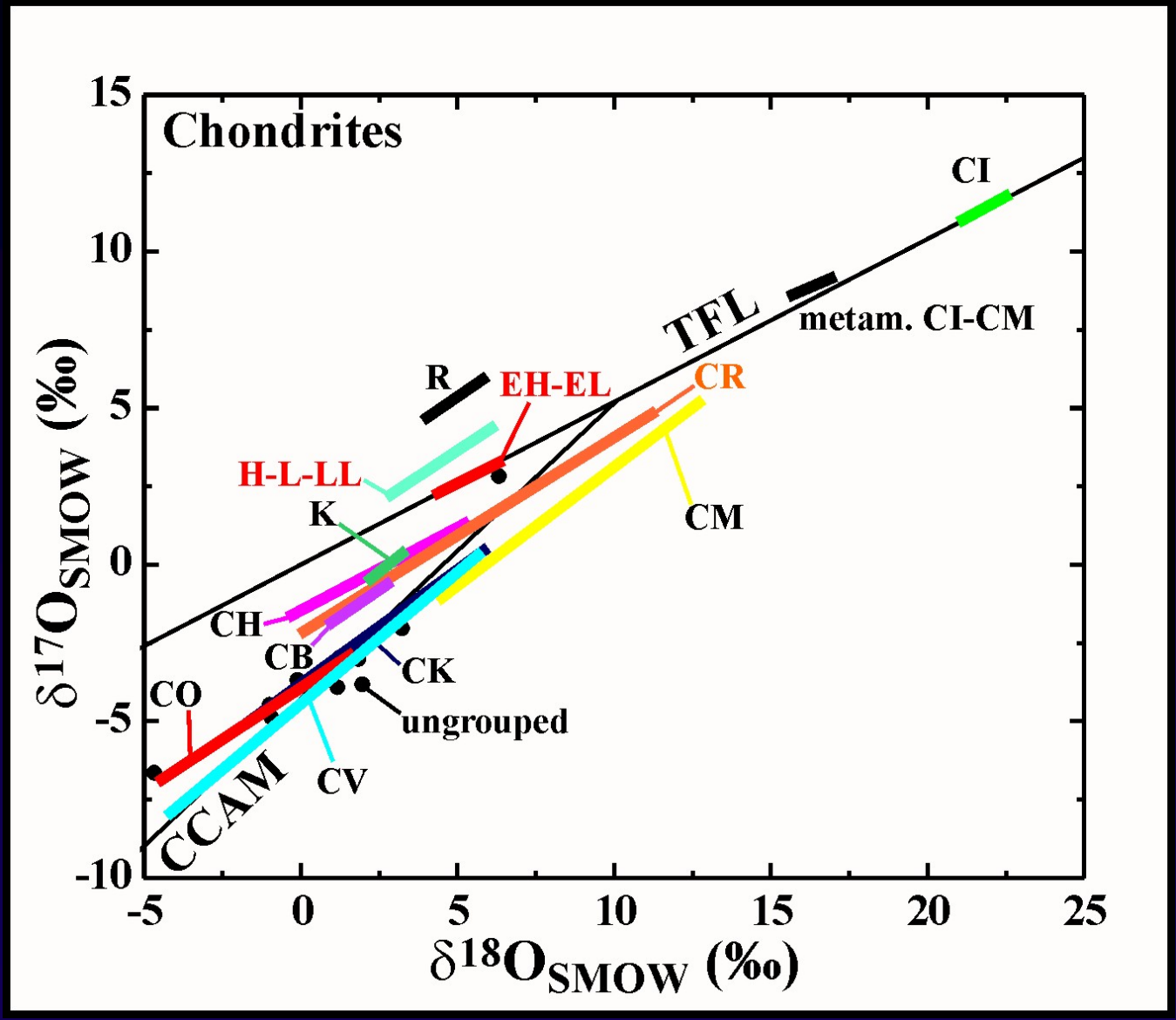

all data from Clayton's lab

$\delta^{17,18}O = [(^{17,18}O/^{16}O)_{sample}/(^{17,18}O/^{16}O)_{SMOW} - 1] \times 1000$, Standard Mean Ocean Water

Classification parameter: Mineralogy & petrography

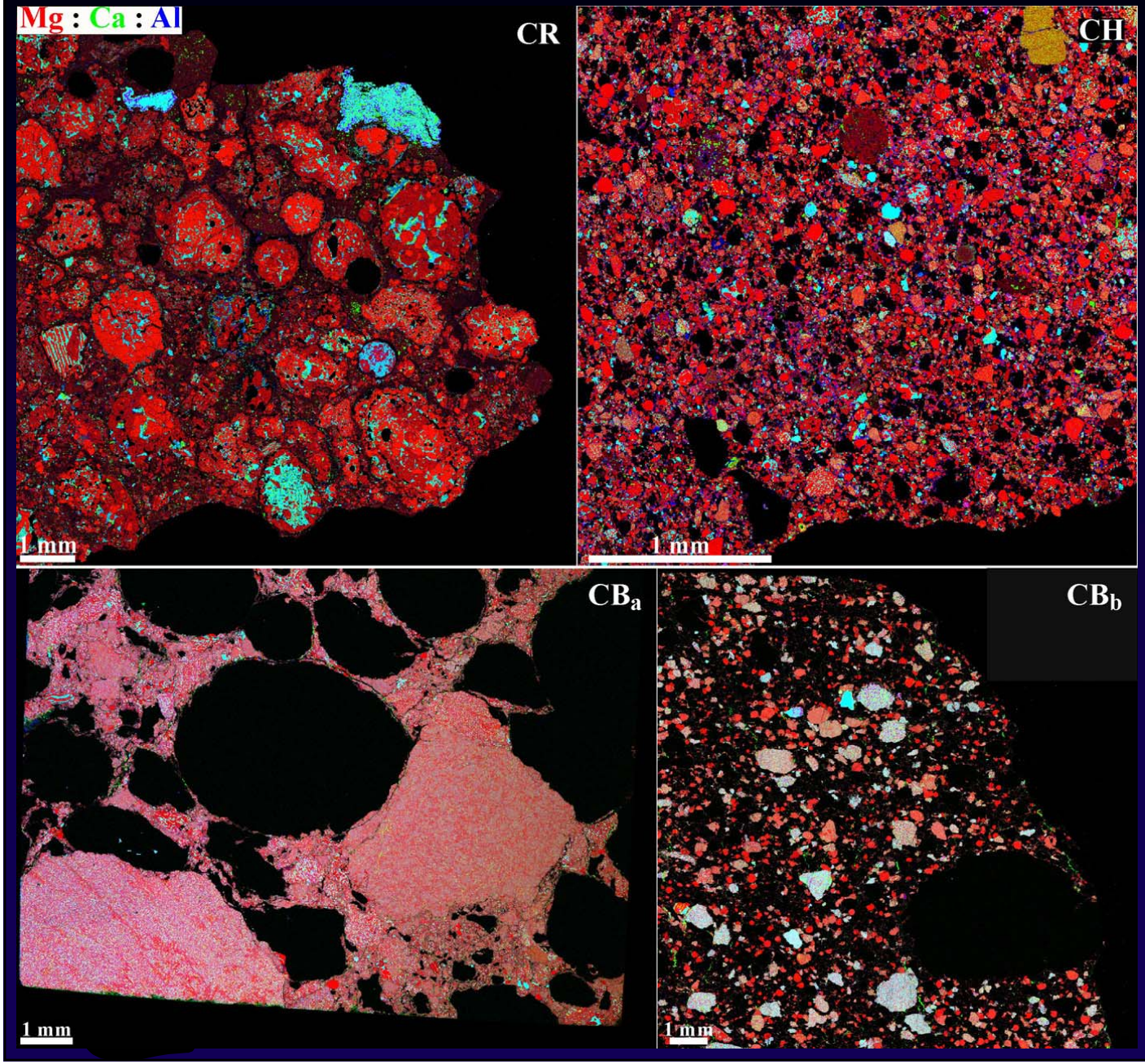

- variations in modal abund. of chondrules, CAIs, metal & matrix
- chondrule textures & compositions

Classification parameter: Mineralogy & petrography

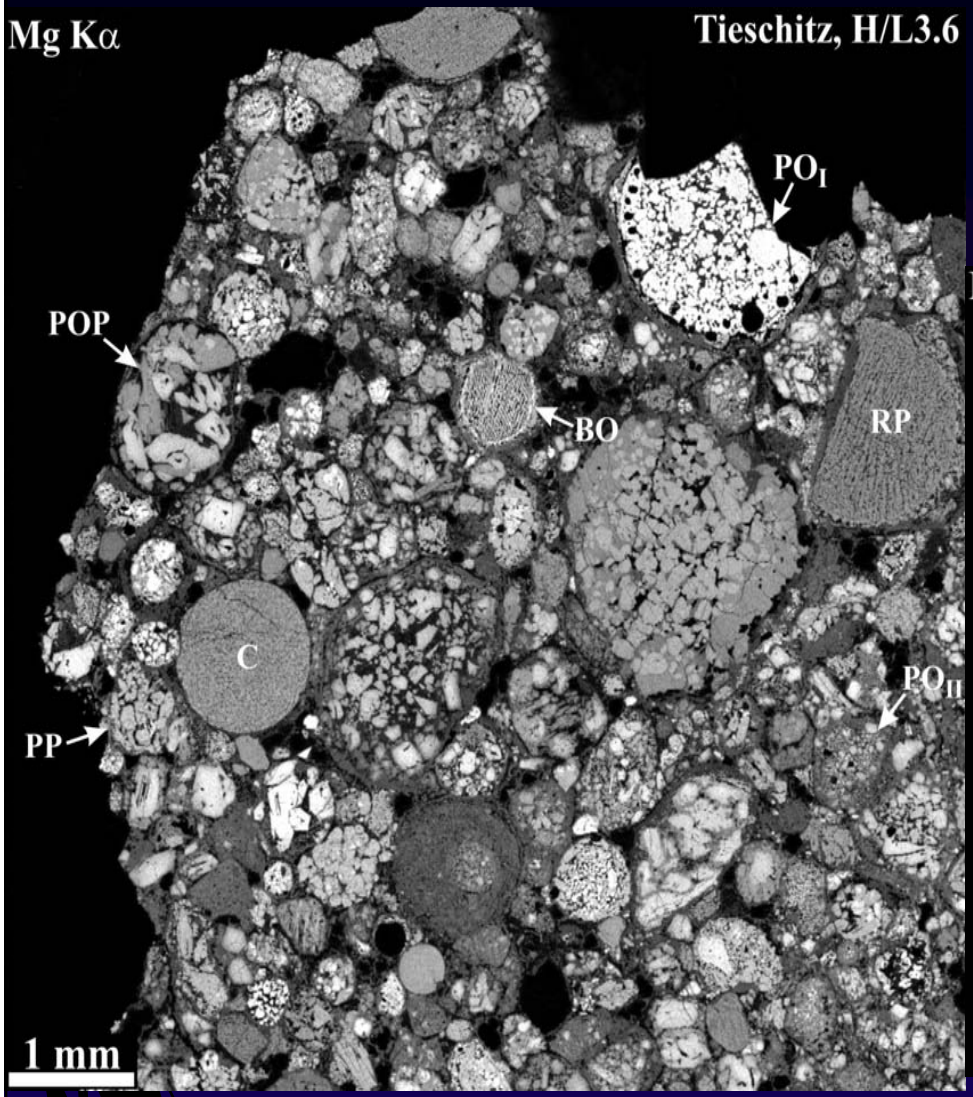

- variations of chondrule textures & compositions

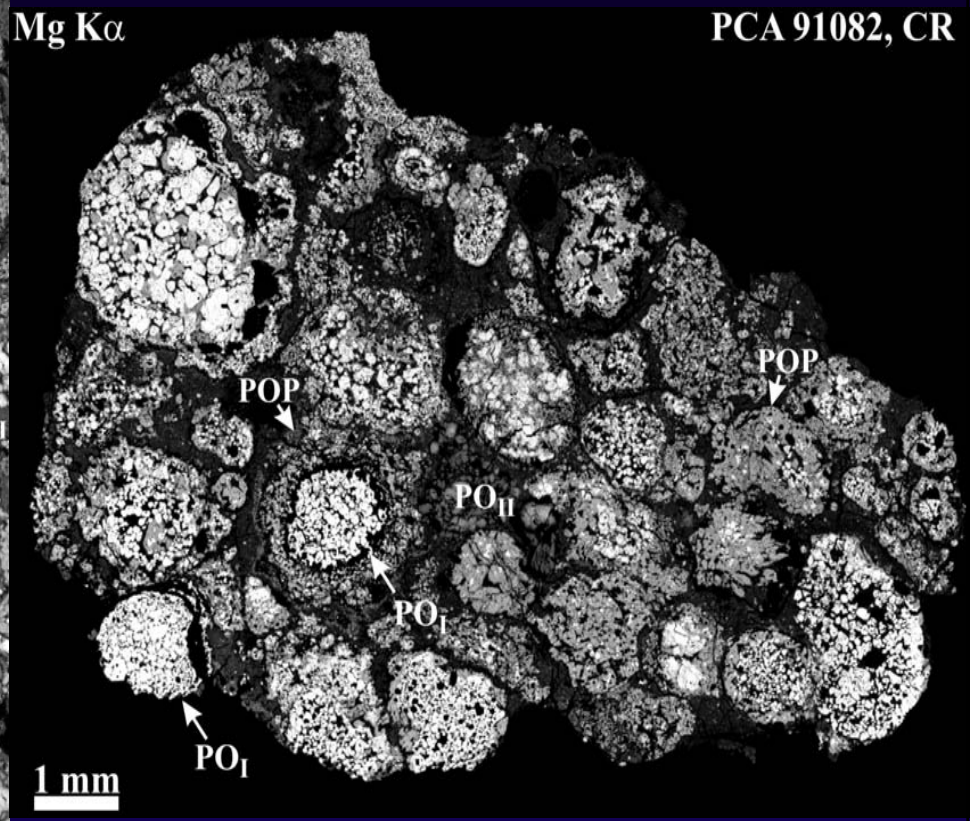

CVs: *oxidized* Allende-like & Bali-like & *reduced* subgroups

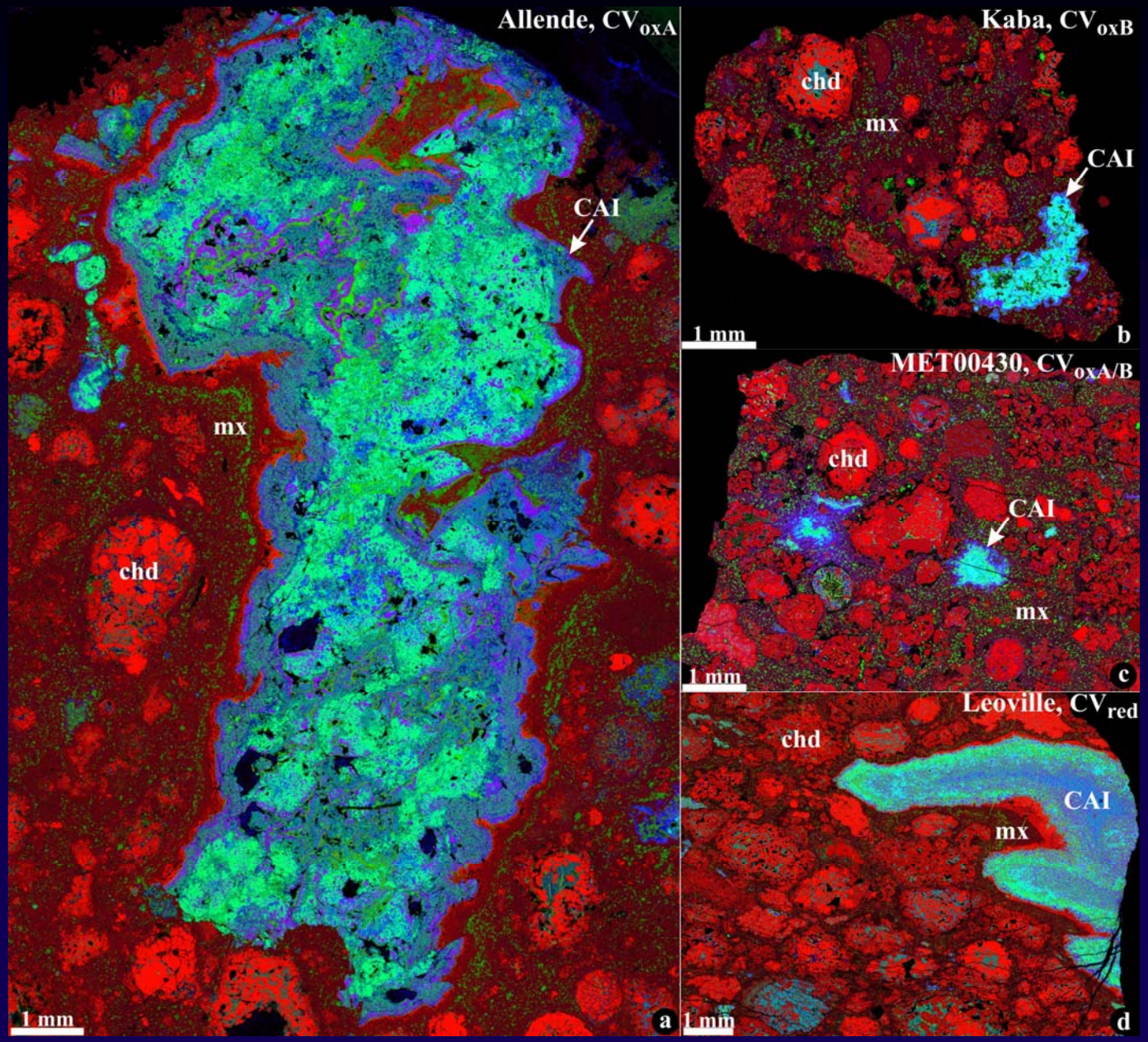

- CV subgroups may reflect postaccretionary alteration processing

CB chondrites: *CB_a & CB_b subgroups*

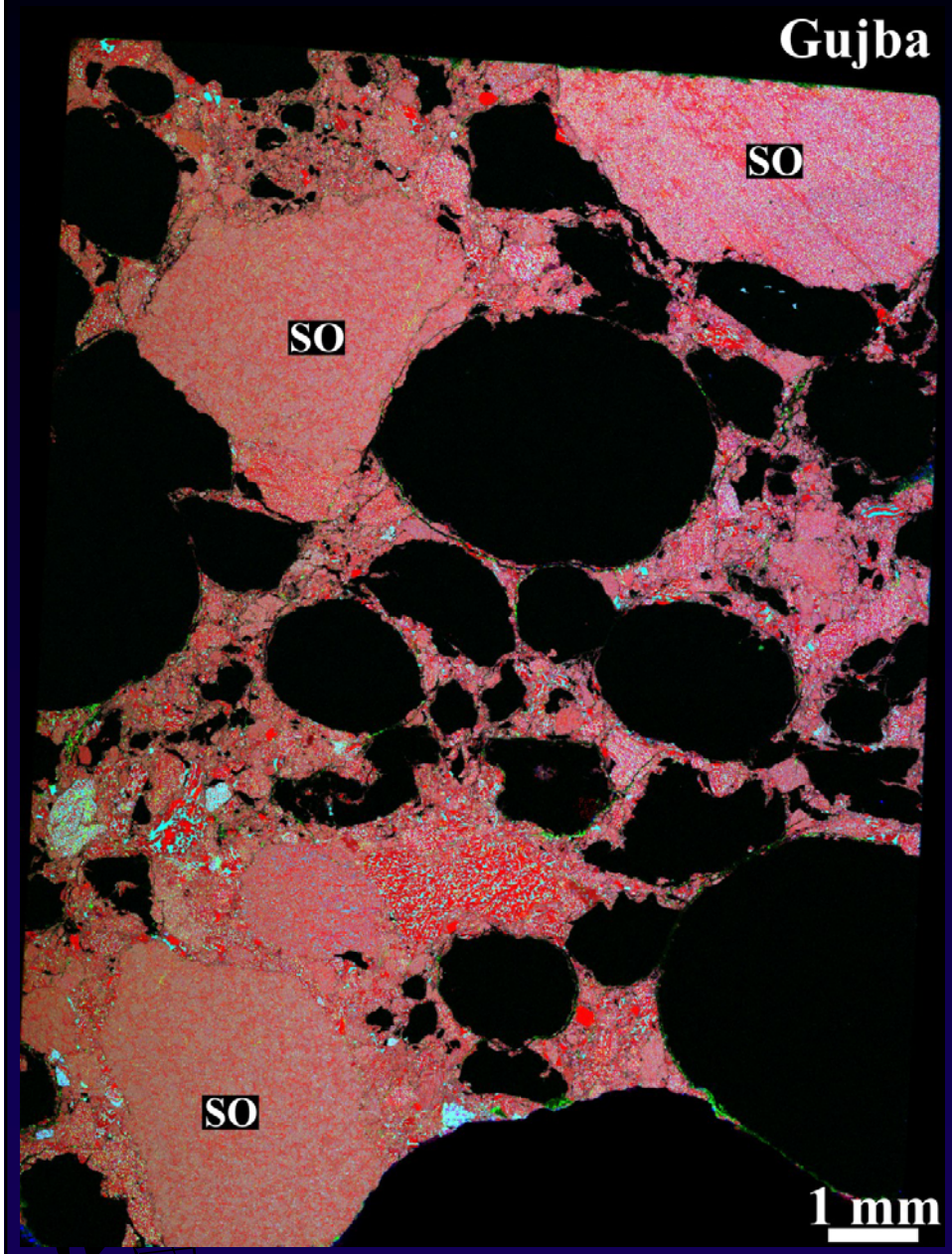

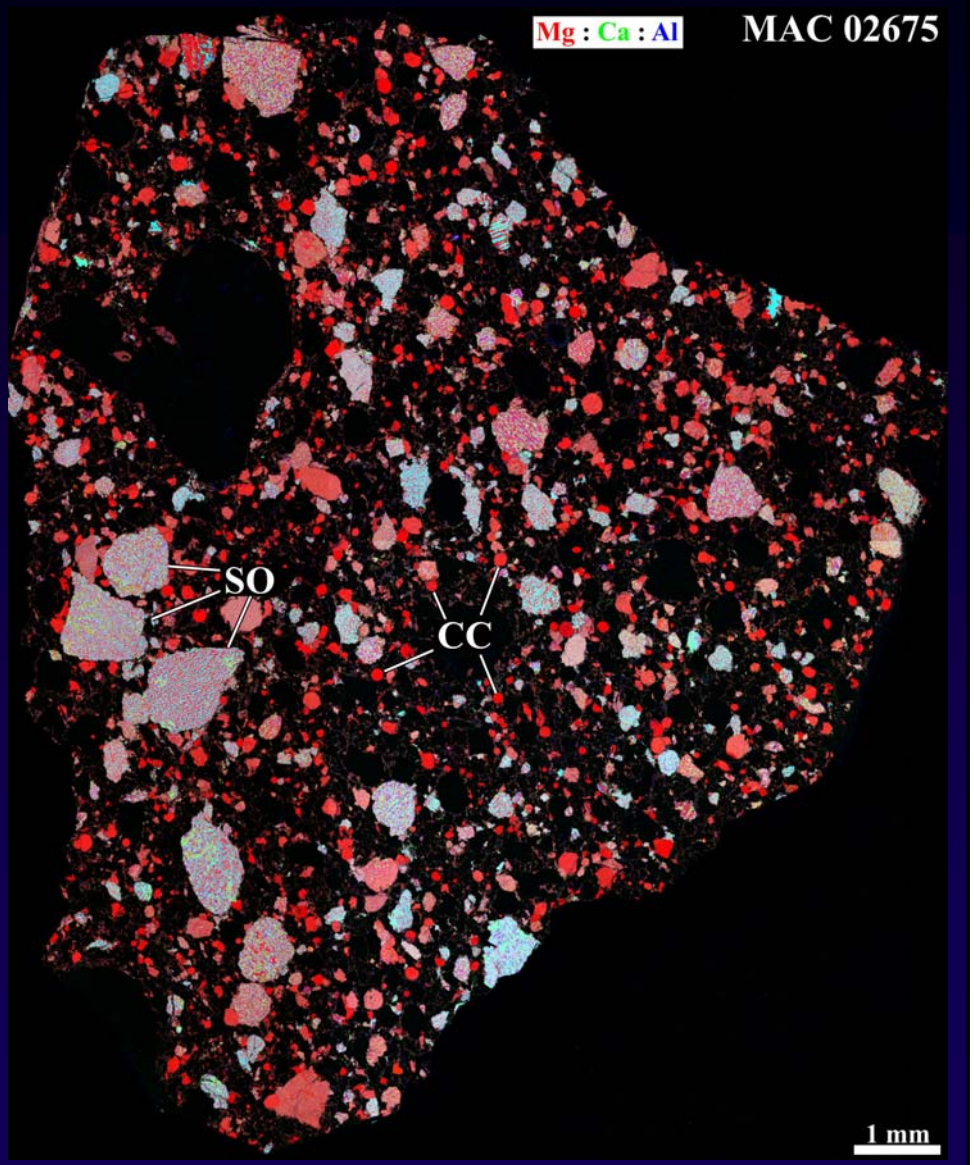

CB chondrites: *CB_a & CB_b subgroups*

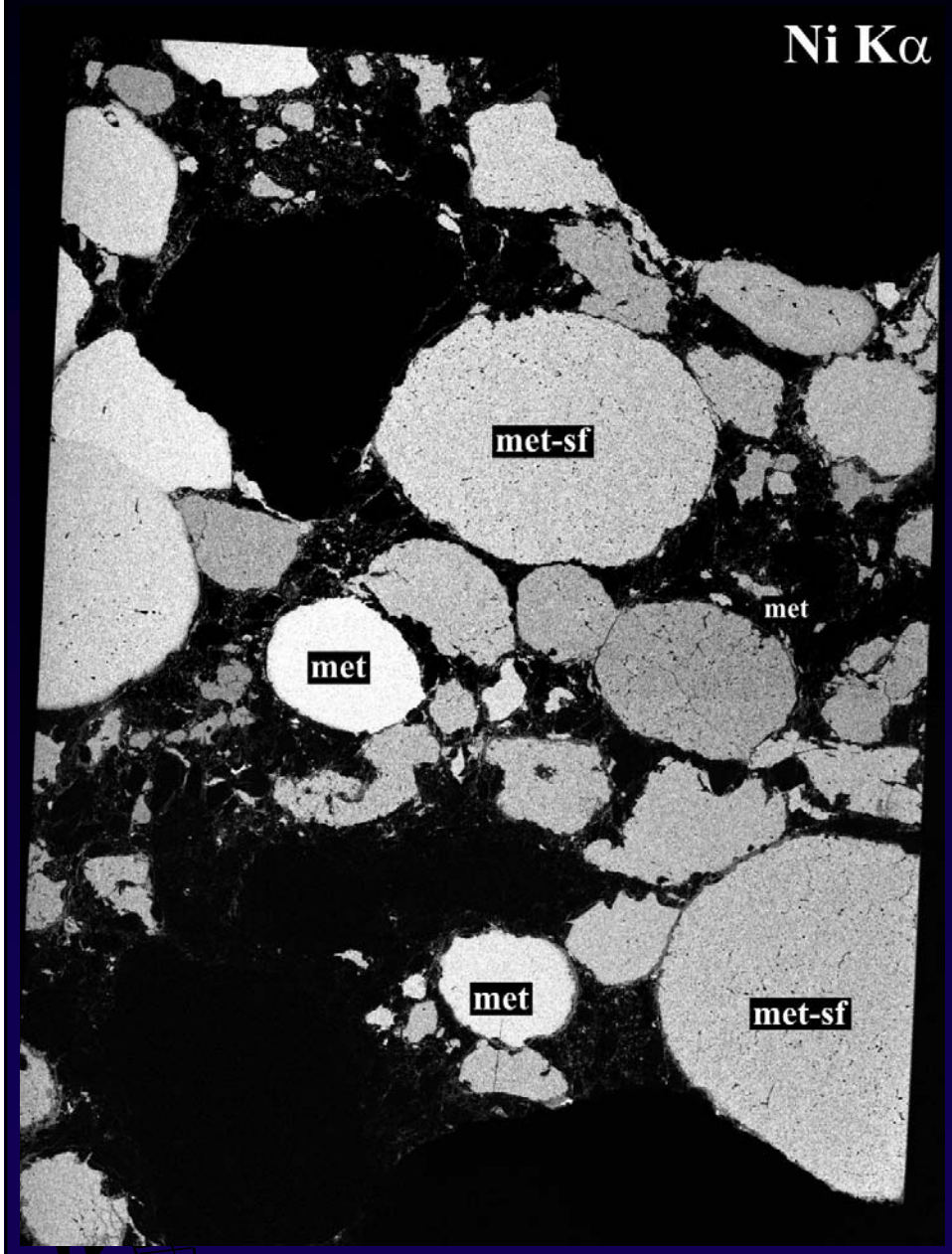

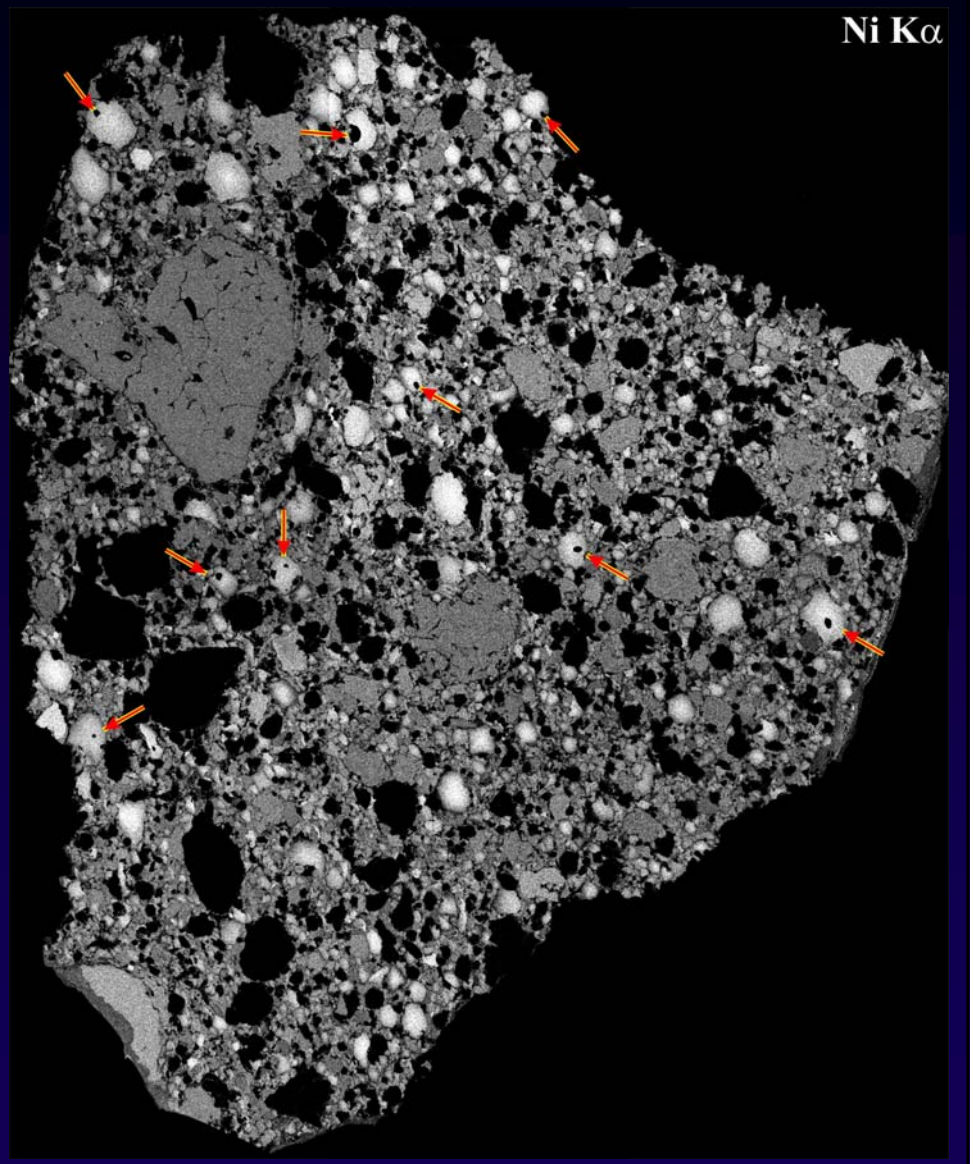

- CB subgroups reflect primary accretionary processes

Not all carbonaceous chondrites are C-rich

- term *"carbonaceous"* is somewhat misnomer: only CI, CM, & CR chondrites are enriched in C relative to noncarbonaceous chondrites

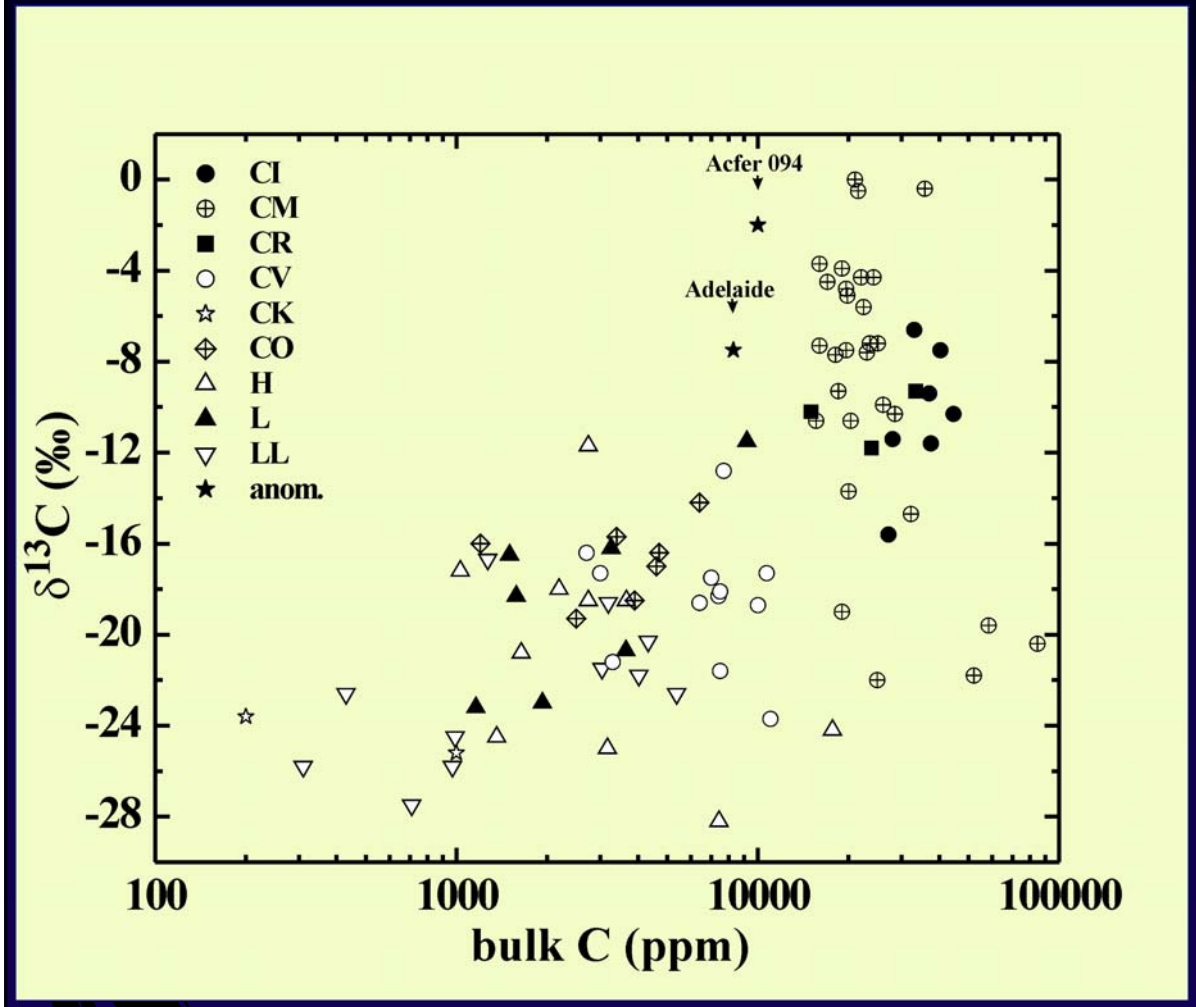

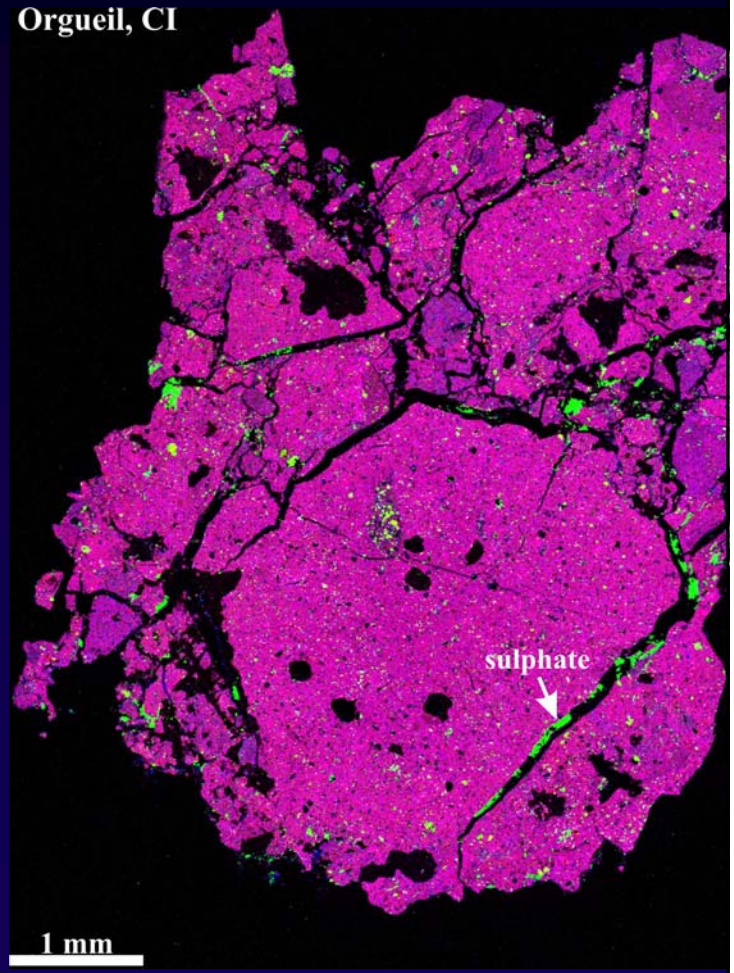

CC *vs.* nonCCs: O-isotopic differences

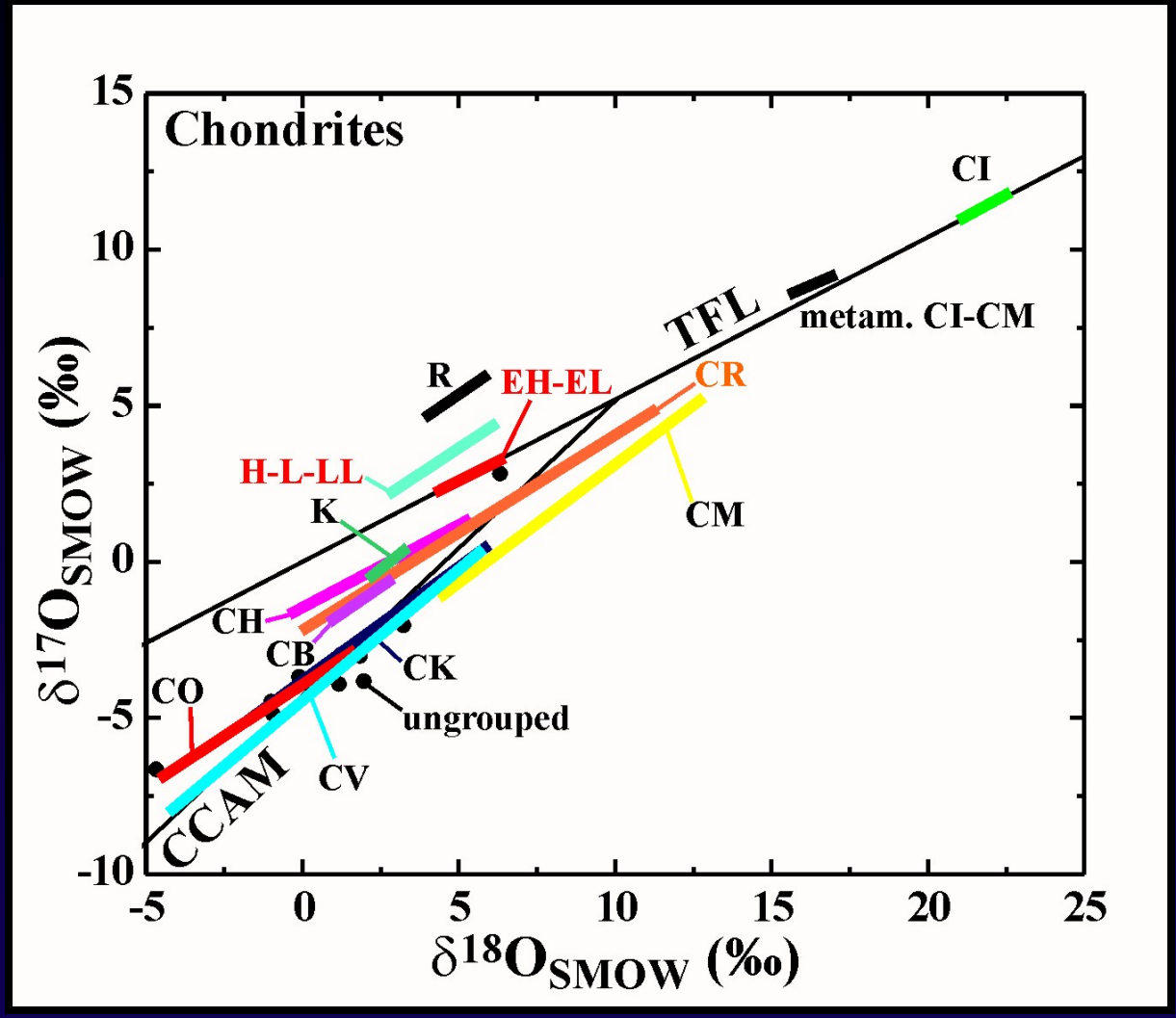

all data from Clayton's lab

- O-isotopic compositions of CCs are below TFL (except CI & metam. CM)
- O-isotopic compositions of nonCCs are above TFL (except K chondrites)

CC *vs.* nonCCs: Mineralogical differences

- matrix/chondrule ratio: ≥0.9 in CCs; ≤0.9 in nonCCs, except CHs & CBs
- CAI abundances: >0.1 vol% in CCs; <0.1 vol% in nonCCs

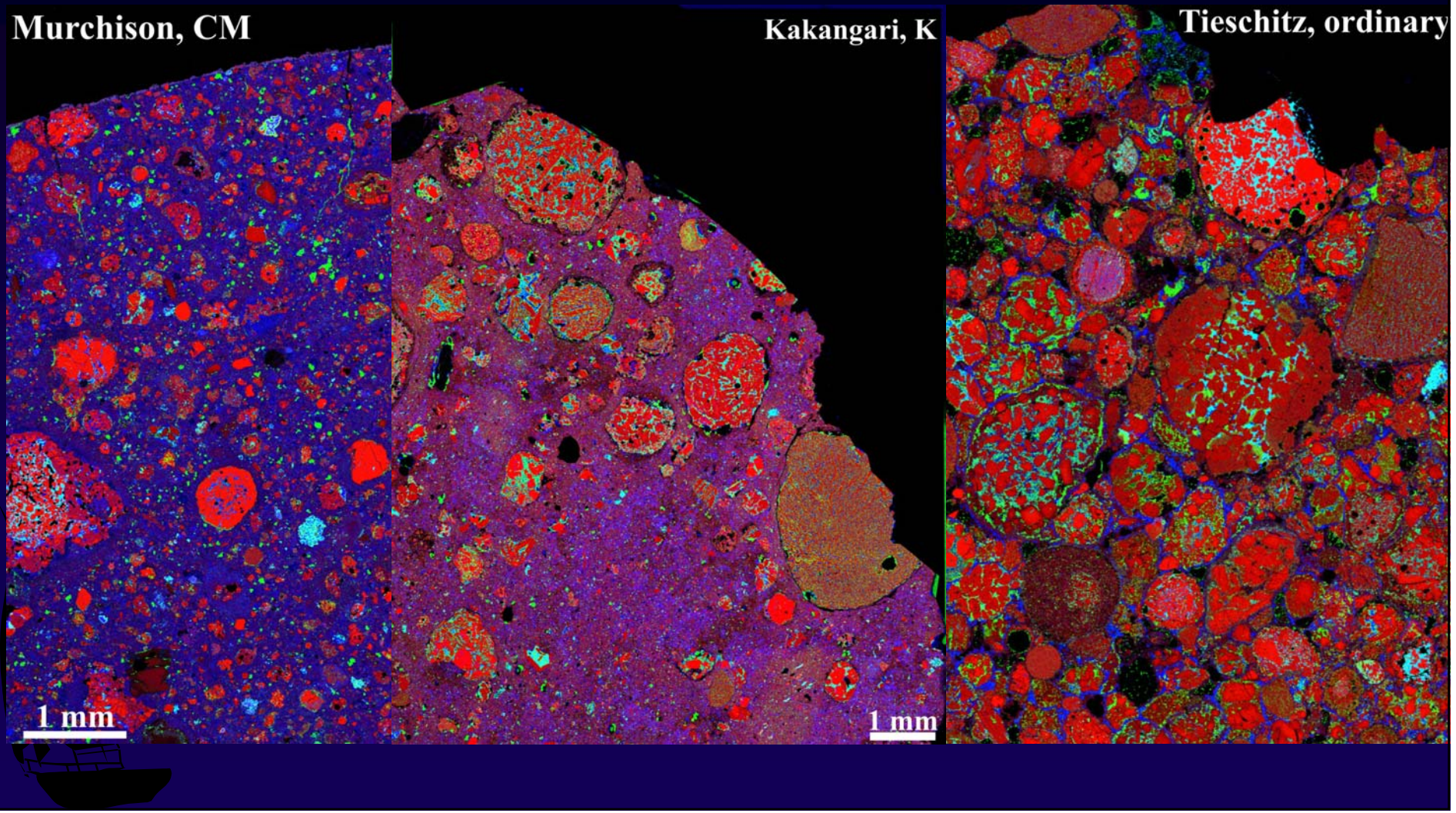

CC *vs.* nonCCs: Chemical differences

- refractory lithophile/Mg abundance ratios relative to CIs:
  ≥ 1.0 in CCs; ≤0.95 in nonCCs

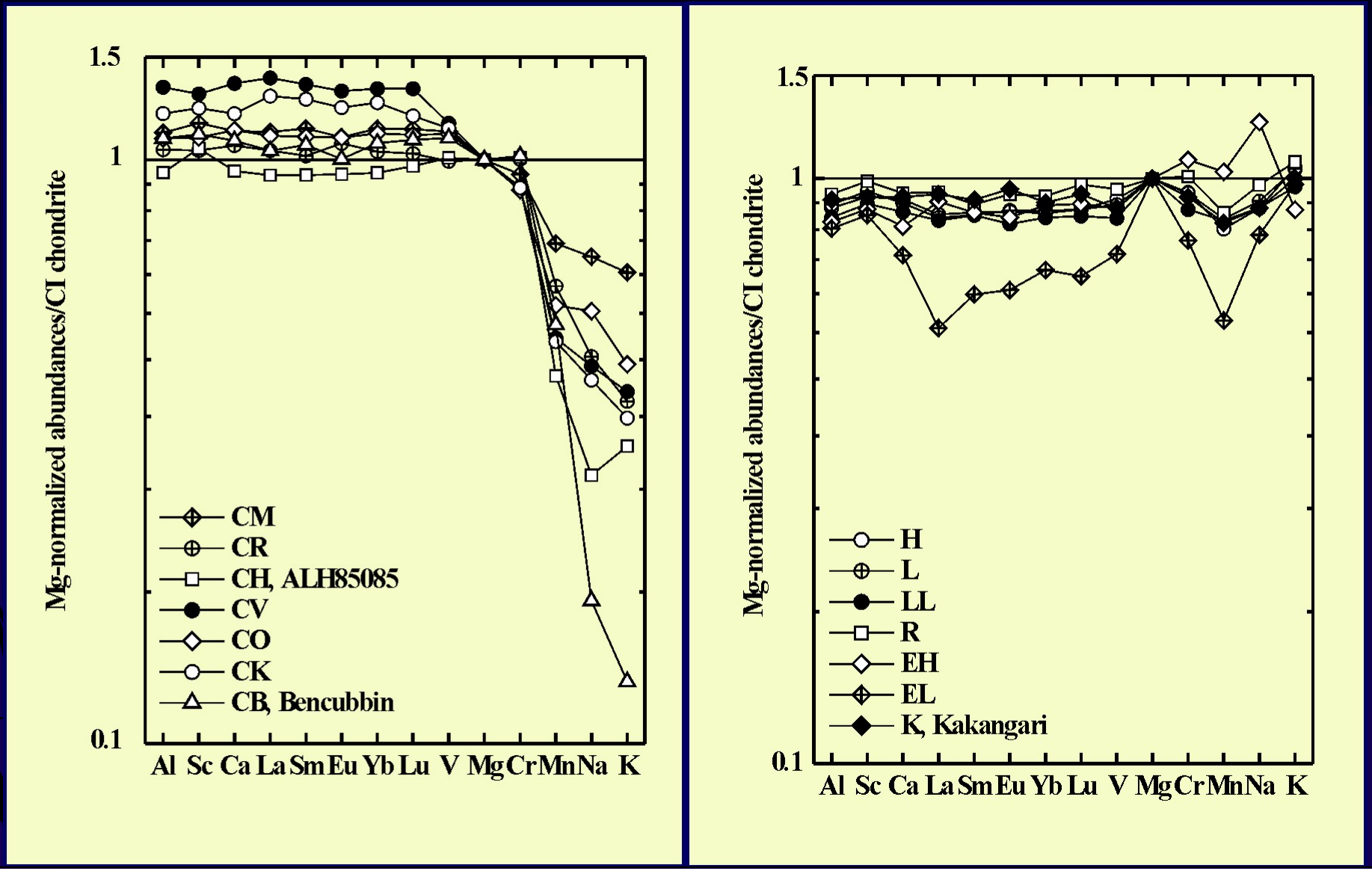

Secondary classification parameters

- Each chondrite group is considered to have sampled a separate asteroid
- Chondrites experienced thermal metamorphism & aqueous alteration on their parent asteroids (*Adrian Brearley*)
- Van Schmus & Wood (1967) divided chondrites into petrographic types 1-6

Chondrites

class →	**Carbonaceous**								**Ordinary**			**Enstatite**		
group →	**CI**	**CM**	**CO**	**CR**	**CB**	**CH**	**CV**	**CK**	**H**	**L**	**LL**	**EH**	**EL**	**R**	**K**
petr. type →	**1**	**1-2**	**3-4**	**1-2**	**3**	**3**	**3-4**	**3-6**	**3-6**			**3-6**		**3-6**	**3**

- type 3 are called unequilibrated
  - type 3 ordinary, CV & CO chondrites are divided in subtypes (3.0-3.9); type 3.0 are considered the most primitive chondrites
- type 4-6 are equilibrated
  - sequence 3 → 4 → 5 → 6 represents increasing degree of chemical equilibrium & textural recrystallization during thermal metamorphism
  - type 1 & 2 represent aqueously altered chondrites (CI1, CR2)
  - sequence 3 → 2 → 1 represents increasing degree of aqueous alteration (abundance of phyllosilicates)

Petrologic types: H3-6

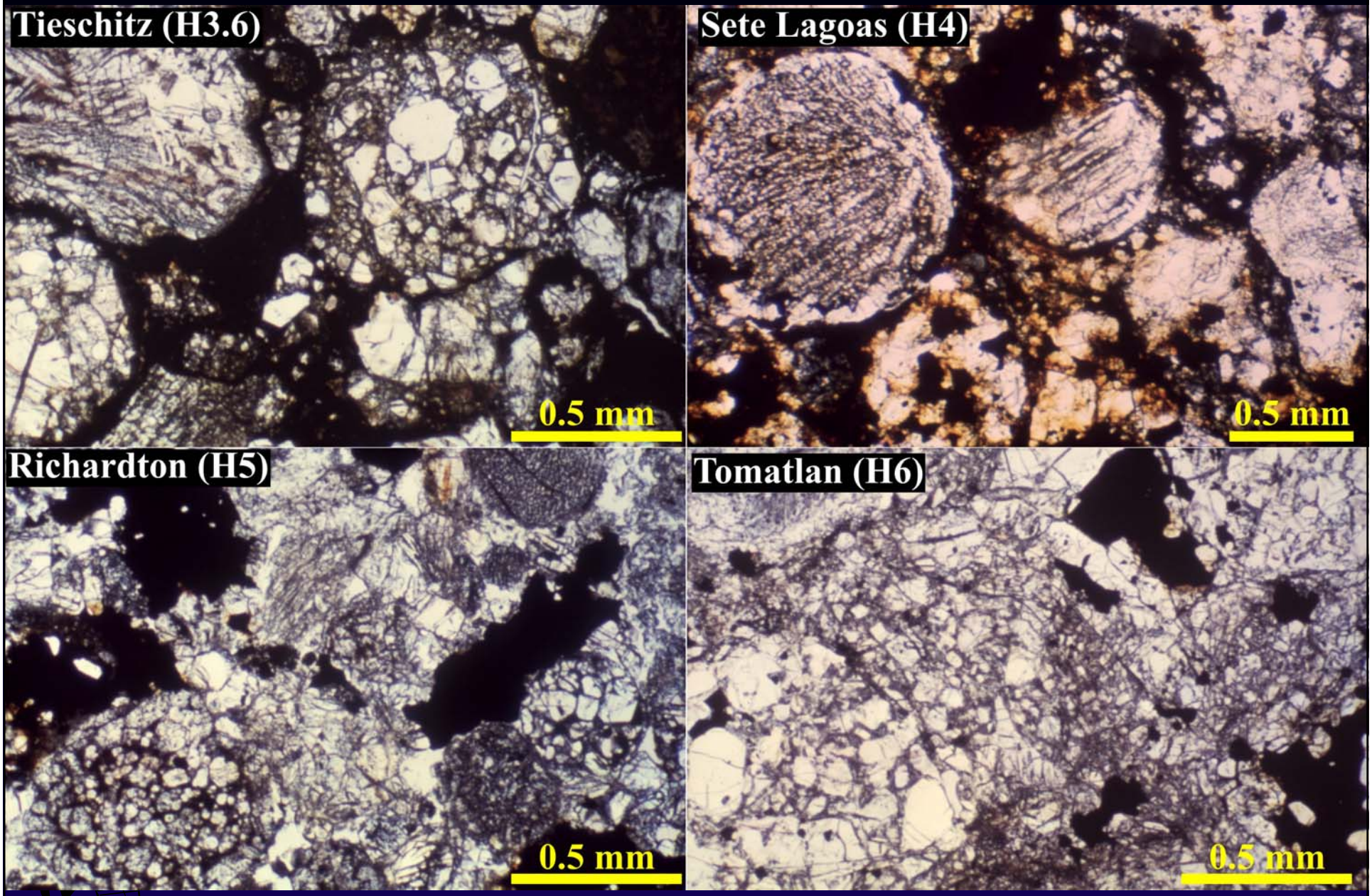

Courtesy of G. Huss

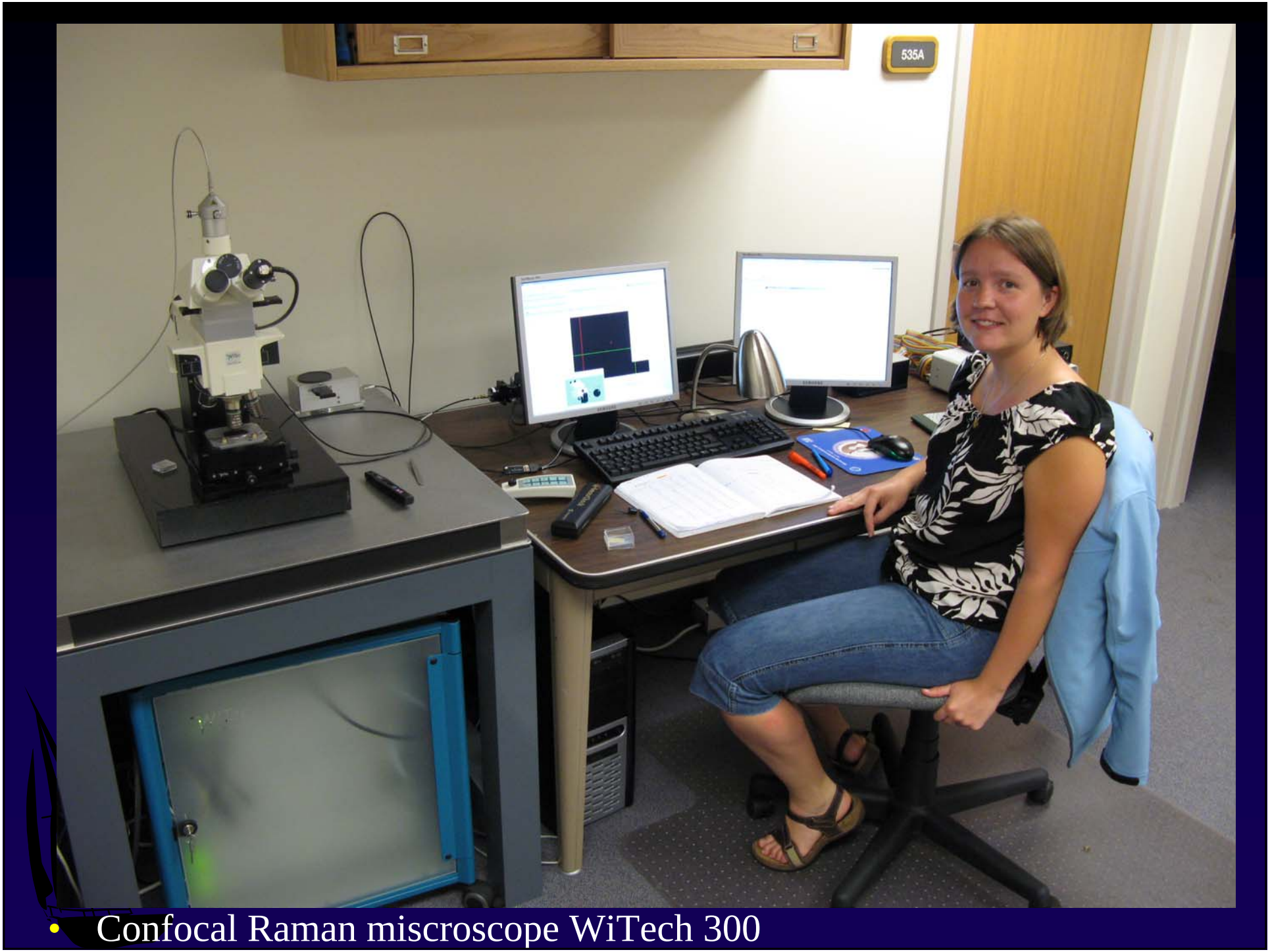

- Confocal Raman miscroscope WiTech 300

Use of Raman spectroscopy for classification of type 3 chondrites

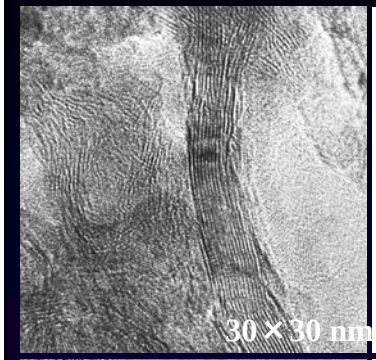

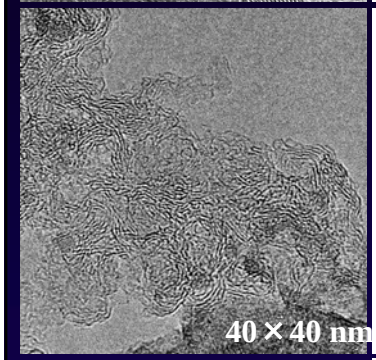

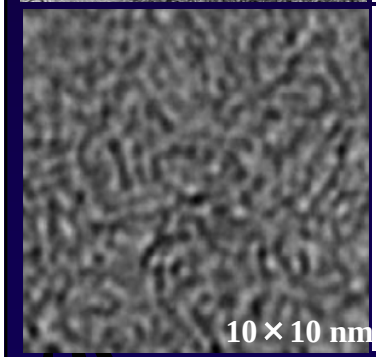

HR-TEM

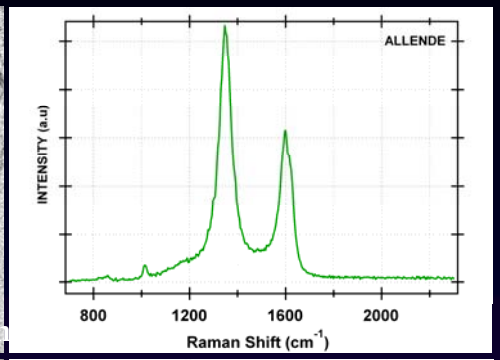

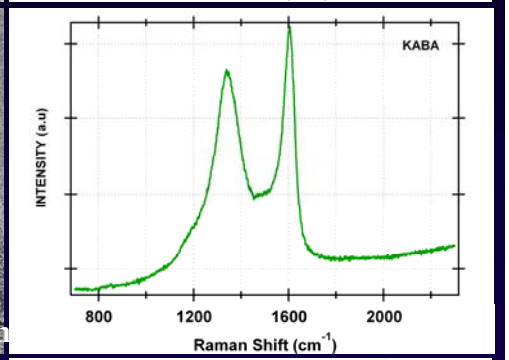

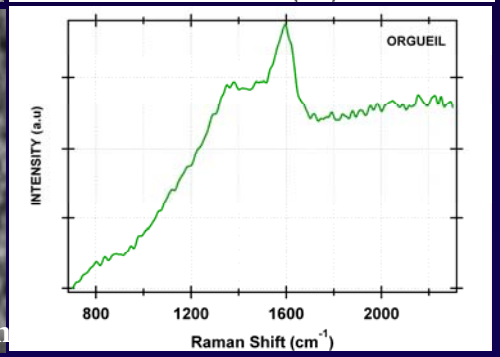

Raman spectra

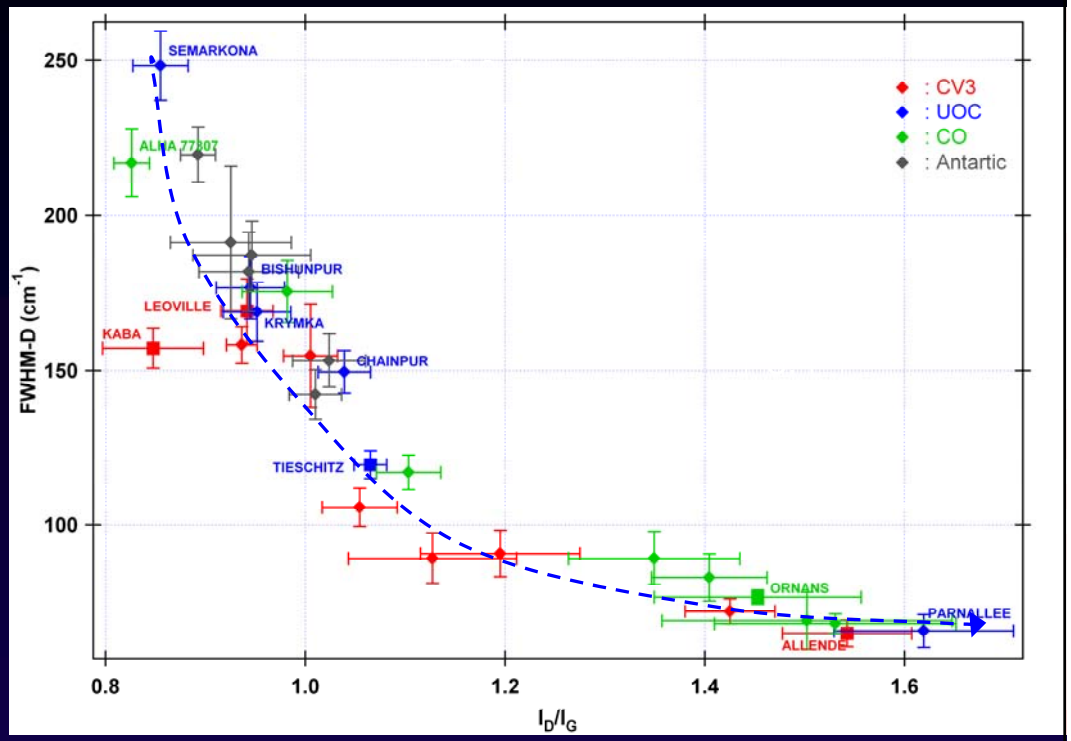

Bonal et al. (2006) GCA

- structural order of the insoluble organic matter is sensitive to thermal metamorphism

Literature

- Krot A.N., Keil K., Goodrich C.A., Scott E.R.D., & Weisberg M.K. (2003) Classification of meteorites. pp. 83-129. In *Meteorites, Comets, and Planets* (ed. A.M. Davis) Vol. 1, *Treatise on Geochemistry* (eds. H.D. Holland & K.K. Turekian), Elsevier-Pergamob, Oxford.
- Weisberg M.K., McCoy T.J., & Krot A.N. (2006) Systematics and evaluation of meteorite classification. pp. 19-53. In *Meteorites and the Early Solar System II* (eds. D.S. Lauretta & H.Y. McSween Jr.), The University of Arizona Press.

Part II. Chondritic components: Major characteristics & origins

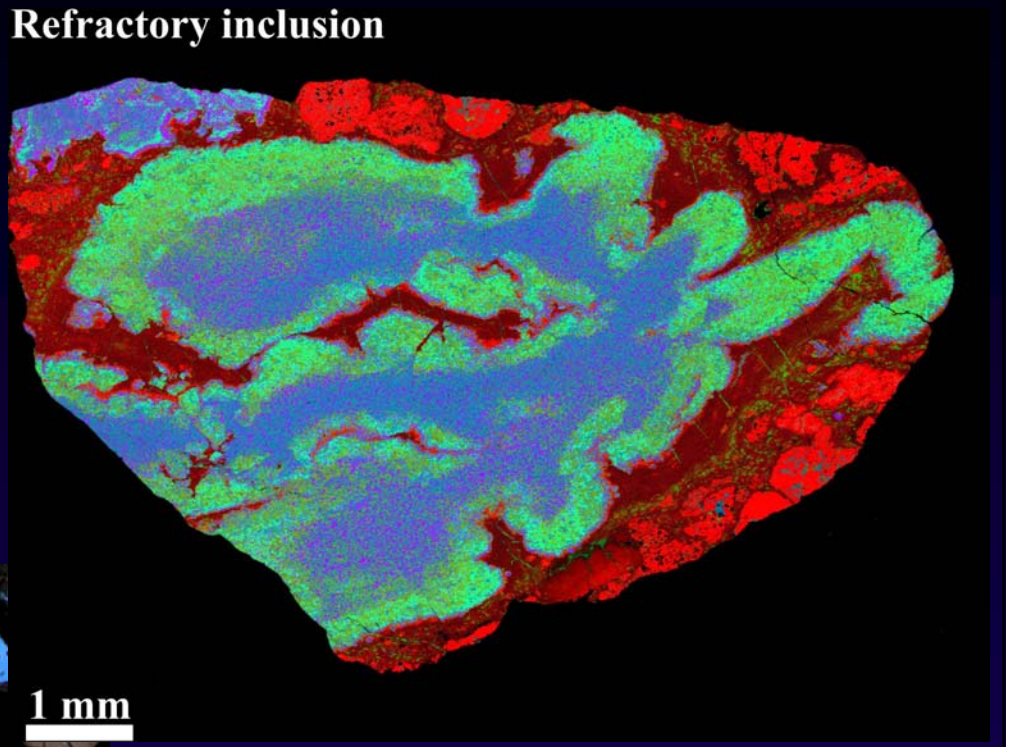

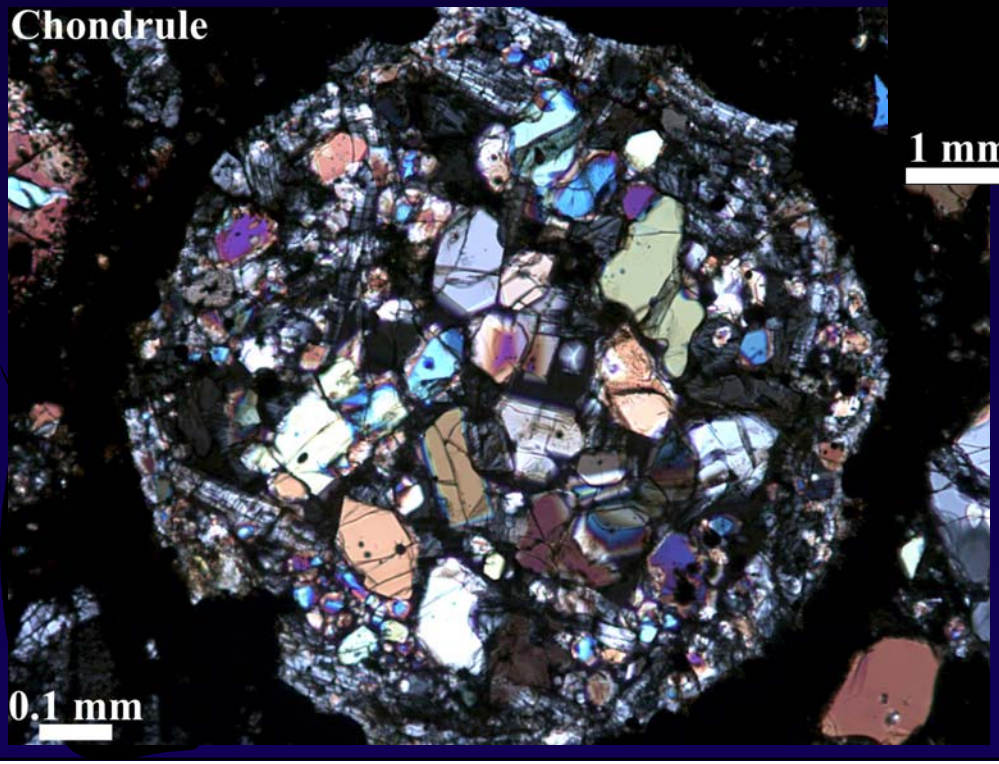

Chondritic components

- refractory inclusions
  - CAIs
  - AOAs
- chondrules
- Fe,Ni-metal
- matrix

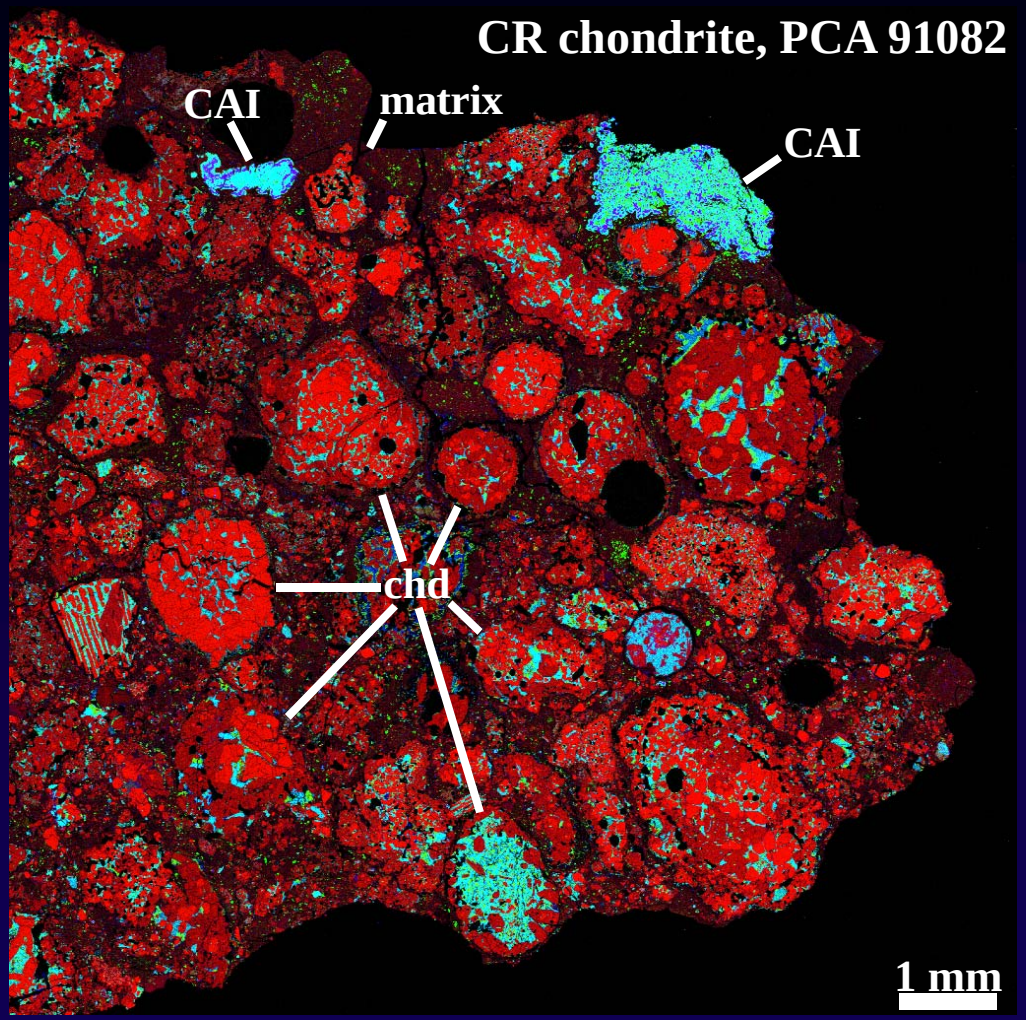

Mineral stability in the solar nebula

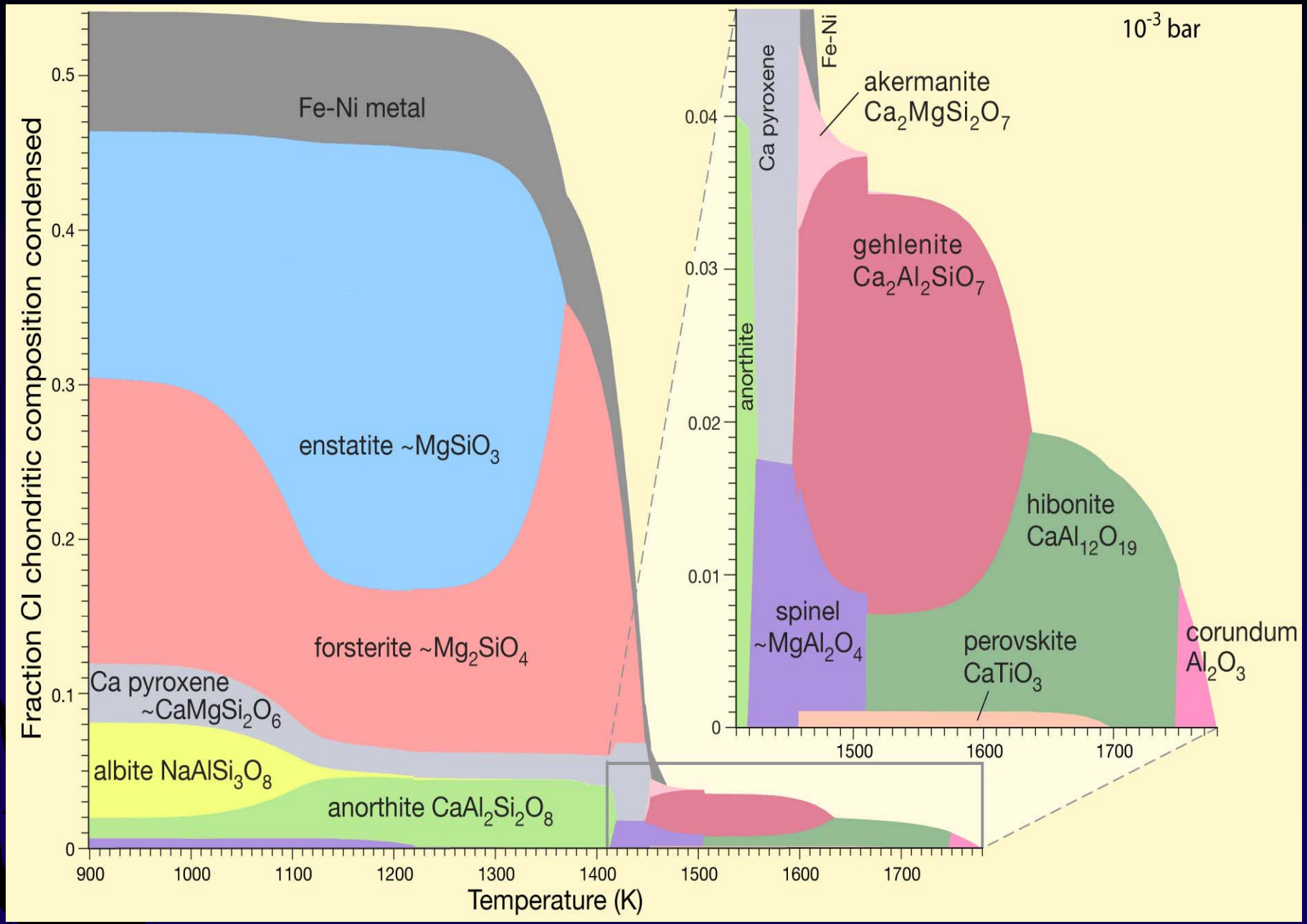

Courtesy of A. Davis

Ca,Al-rich inclusions (CAIs)

- CAIs consist of refractory, crystalline Ca,Al,Ti-minerals with condensation T > 1450 K at $P_{tot} = 10^{-3}$ bar

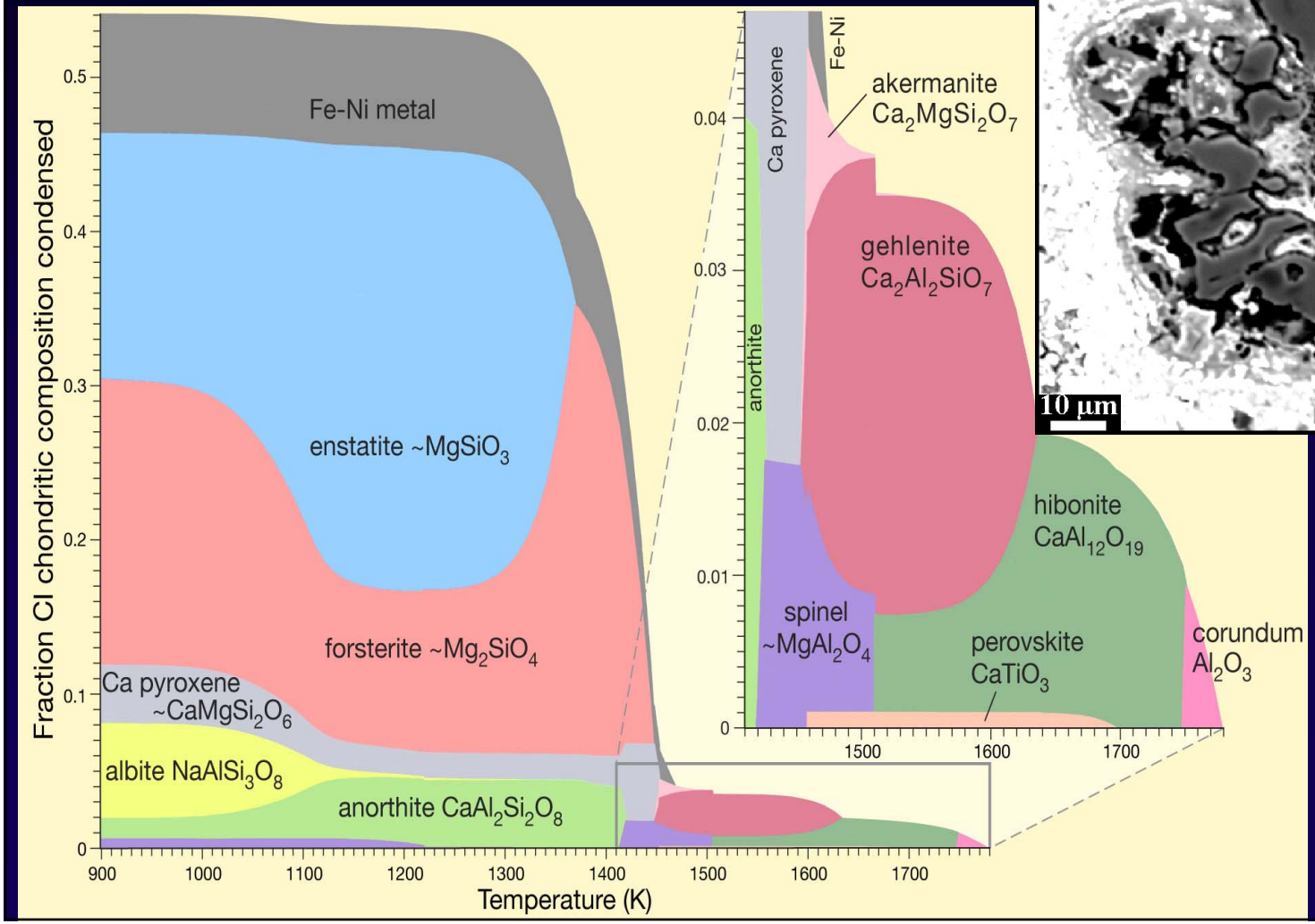

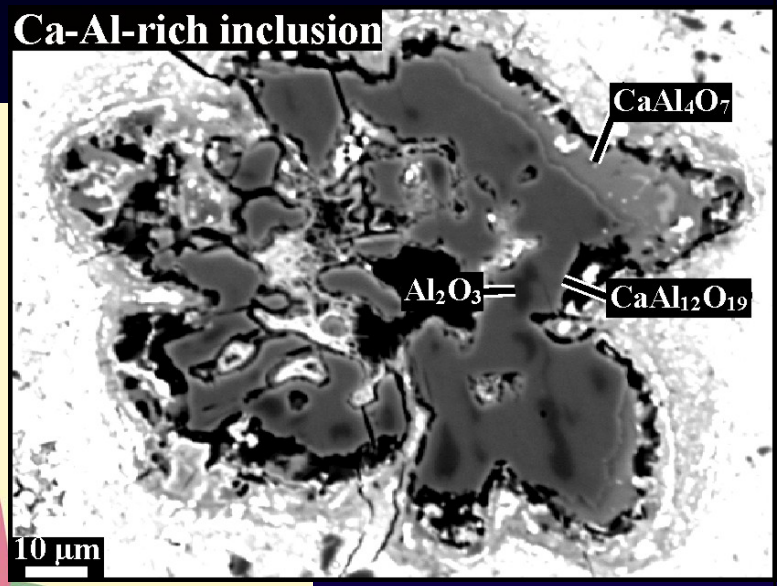

Non-igneous & igneous CAIs

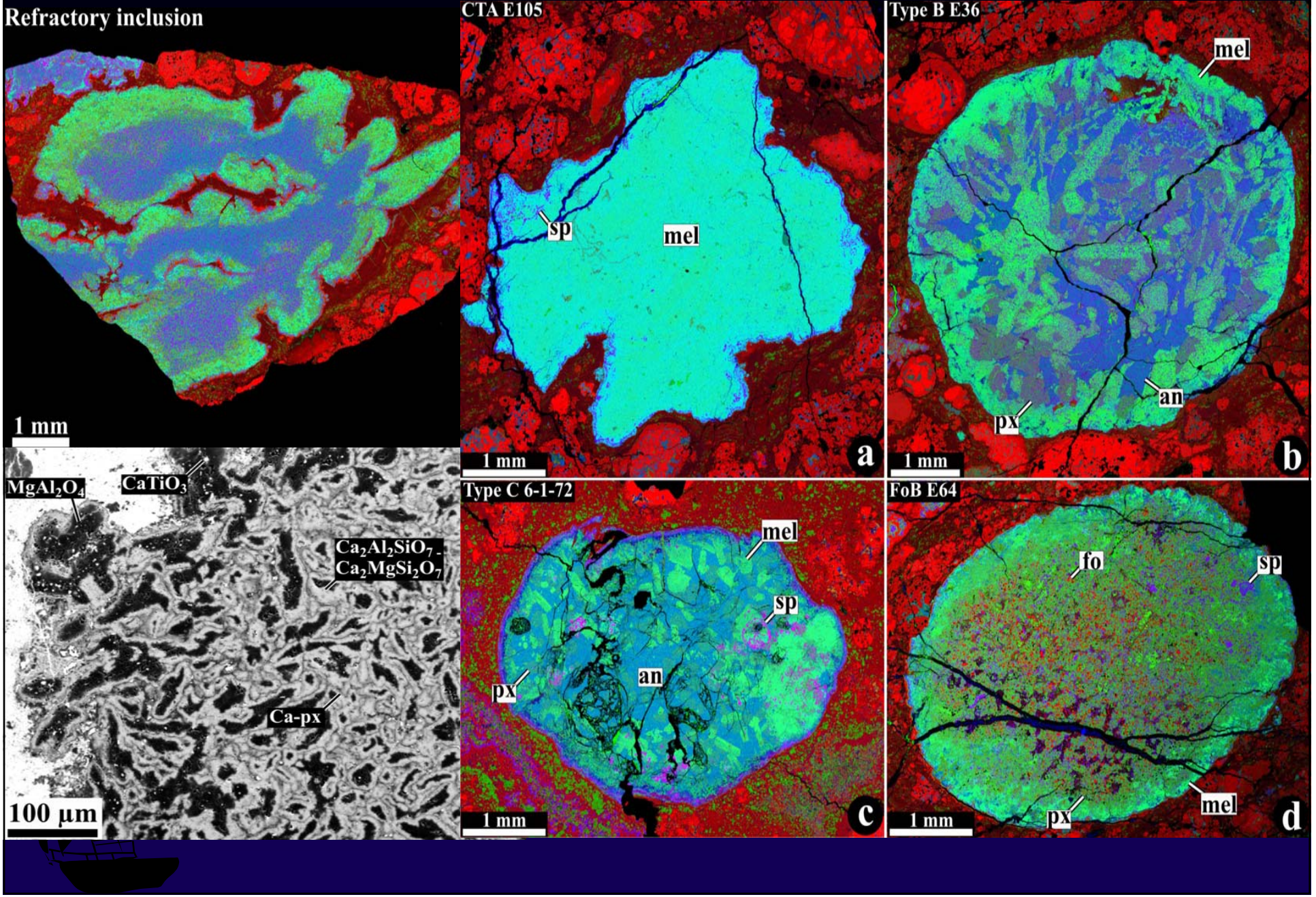

Melted CAIs experienced volatilization

- most CAI melts experienced volatilization which resulted in mass-dependent fractionation of Mg, Si & O isotopes

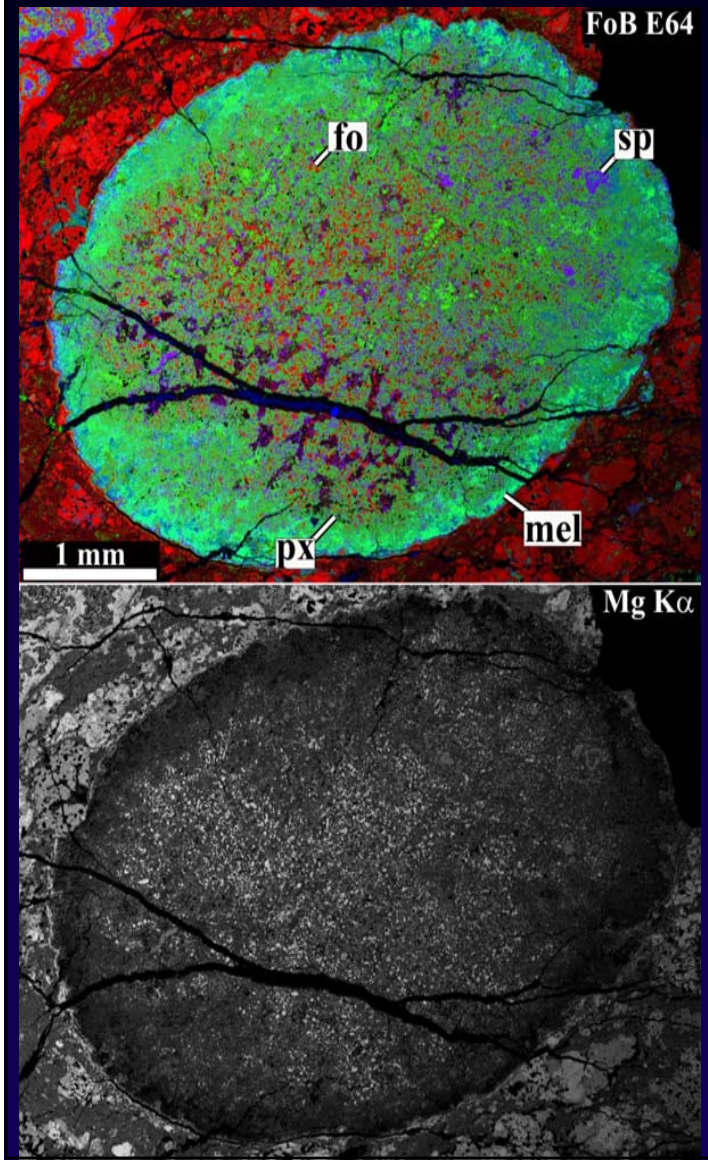

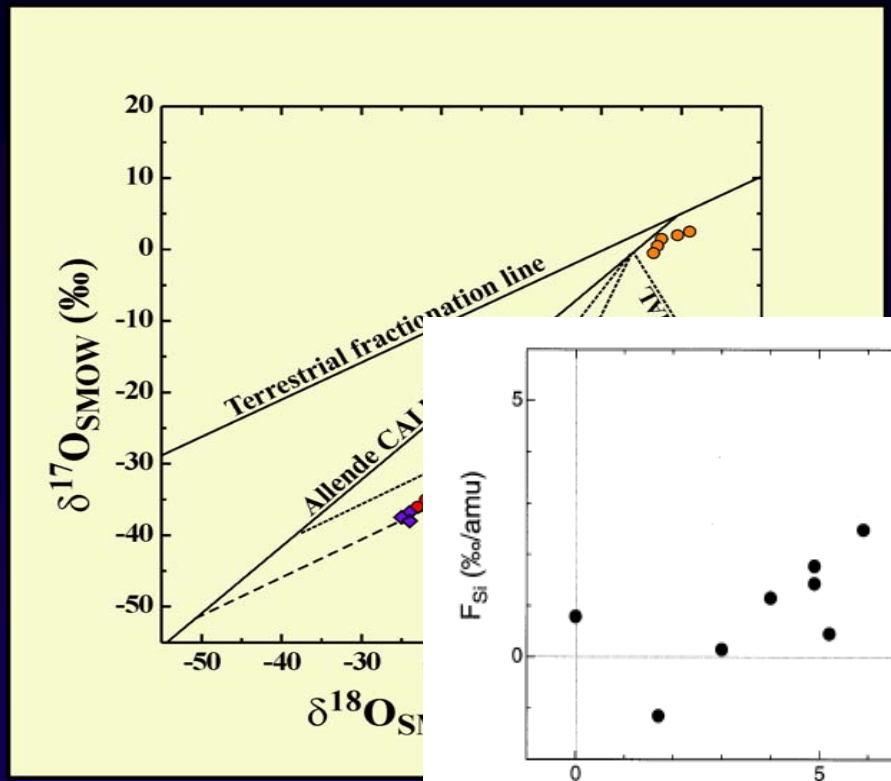

McKeegan et al. (2000) MAPS

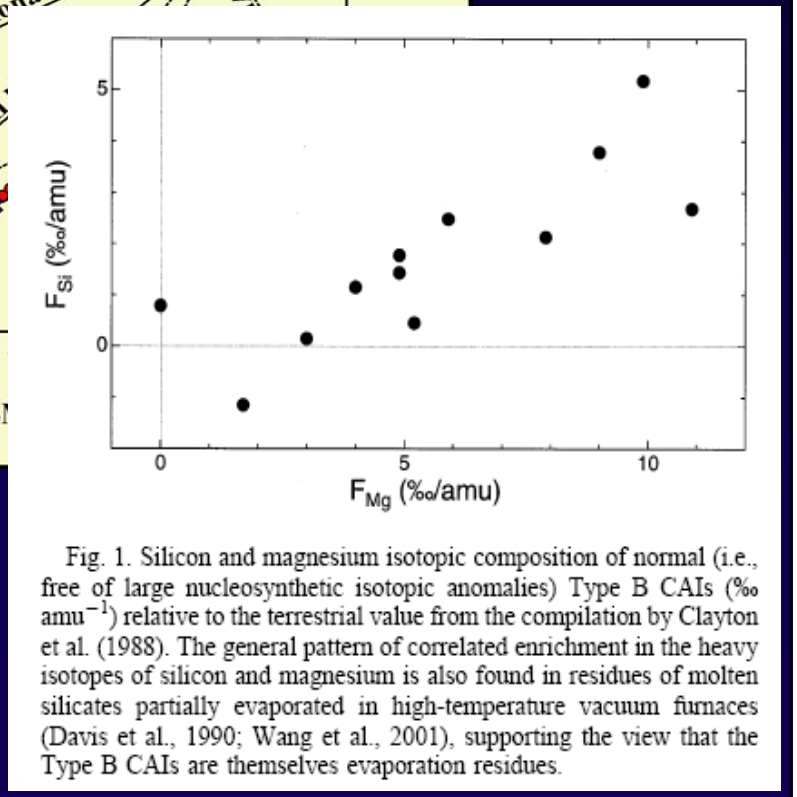

Fig. 1. Silicon and magnesium isotopic composition of normal (i.e., free of large nucleosynthetic isotopic anomalies) Type B CAIs (‰ amu^{-1}) relative to the terrestrial value from the compilation by Clayton et al. (1988). The general pattern of correlated enrichment in the heavy isotopes of silicon and magnesium is also found in residues of molten silicates partially evaporated in high-temperature vacuum furnaces (Davis et al., 1990; Wang et al., 2001), supporting the view that the Type B CAIs are themselves evaporation residues.

Richter et al. (2002) GCA

Experimental constraints on melting of Type B CAIs: *Cooling rates*

- condensation of precursor material from a hot gas of solar composition as it cooled to T ~ 1050-1170˚ C (for P_{H_2} = 10^{-3} – 10^{-5} bar)
- reheating of precursors to ~ 1400˚ C & cooling at 1-50 K/hr
- crystallization & loss of significant fraction of Mg & Si by evaporation

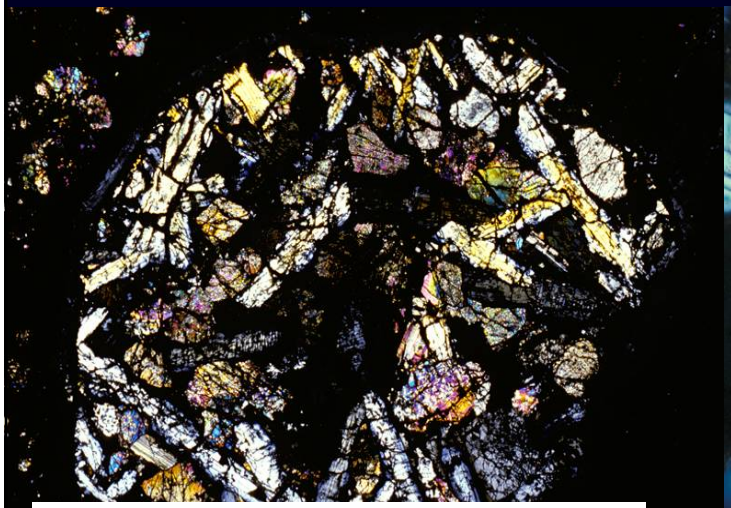

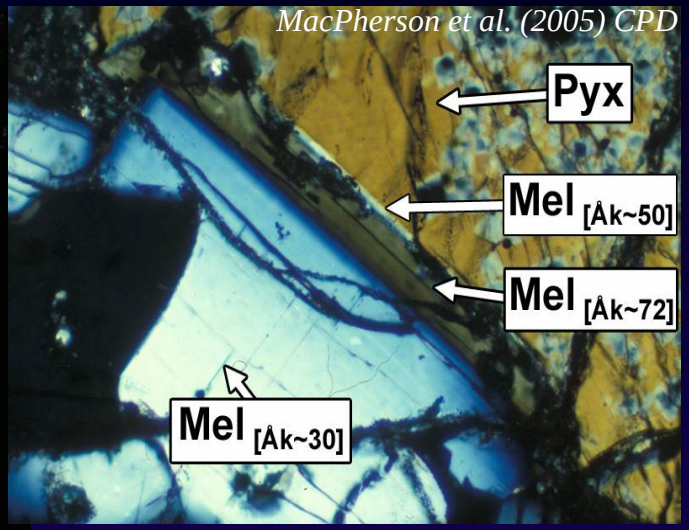

MacPherson et al. (2005) CPD

↓ cooling of CAI melt from 1430˚ C to 1306˚ C at 10˚ C h^{-1} + annealing for 29 hrs & quenching reproduce textures & compositional zoning of melilite grains

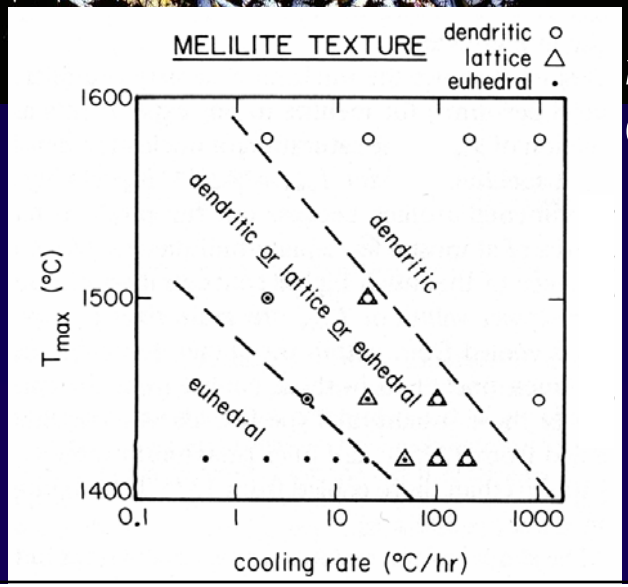

Stolper & Paque (1986) GCA

melilite: solid solution between $Ca_2MgSi_2O_7$ & $Ca_2Al_2SiO_7$

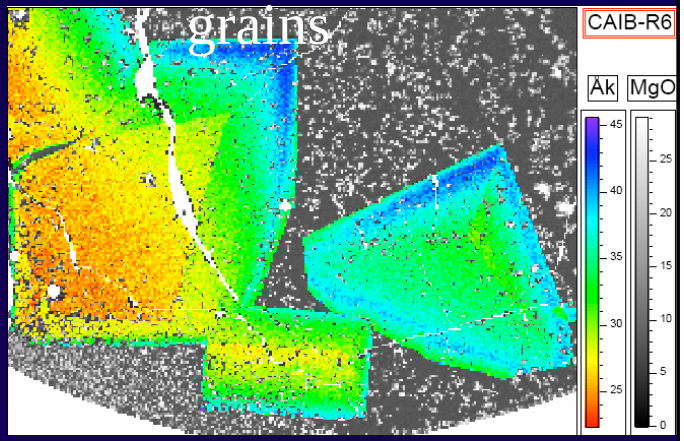

Mendybaev et al. (2006) GCA

Experimental constraints on melting of Type A & Type B CAIs: *Bulk chemical compositions*

- Bulk compositions of igneous CAIs are depleted in Si & Mg compared to the calculated compositions of condensates
- such depletions can be explained by non-equilibrium evaporation into H_2 gas at 1700 K from melt droplets with compositions on a condensation trajectory

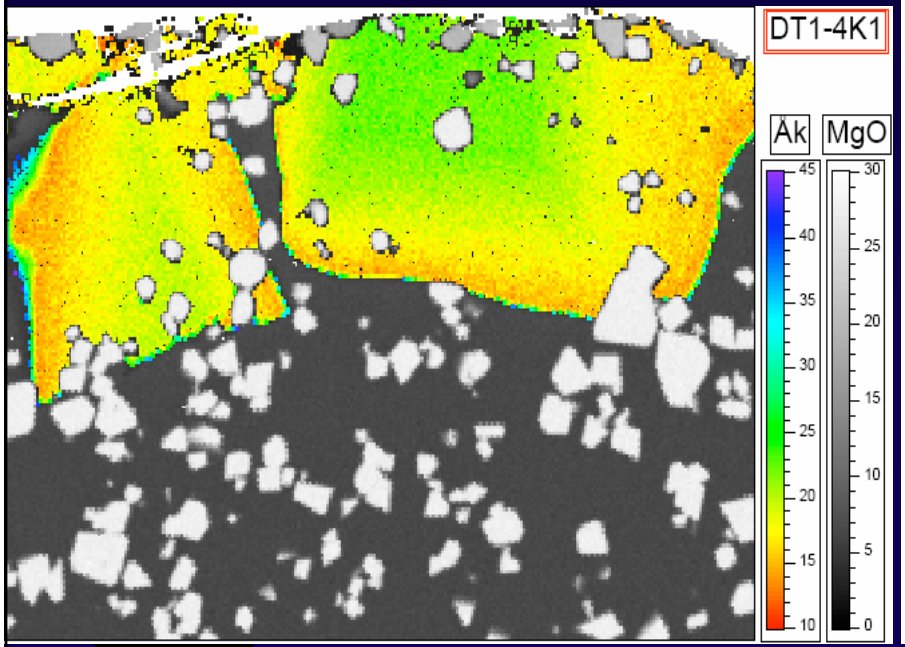

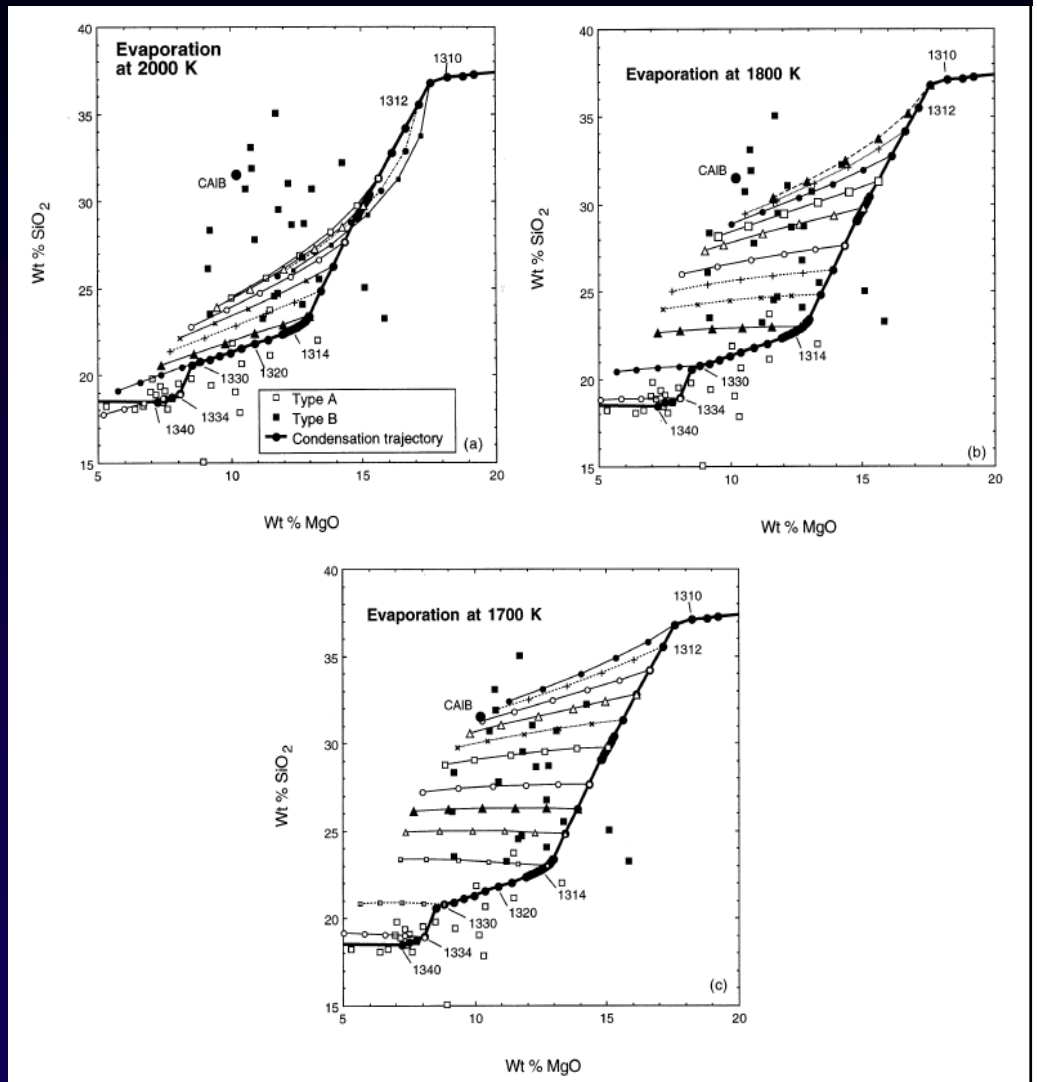

Fig. 9. Comparison between refractory inclusion compositions and those lying along evaporation paths computed at (a) 2000 K; (b) 1800 K; and (c) 1700 K originating from the compositions of equilibrium assemblages of condensates formed in a solar gas at $P^{tot} = 1 \times 10^{-5}$ bar. CAIB is the composition whose liquid–crystal phase relations were studied by Stolper (1982). Compositions along the condensation trajectory are labelled by the temperatures at which they were produced. Evaporation paths emanating from different starting compositions along the condensation trajectory are represented by different symbols. The symbols along the evaporation paths mark compositions produced at increments of 10% of the initial Mg evaporated, from 10% closest to the condensation trajectory to 50% furthest away.

Grossman et al. (2000) GCA

Experimental constraints on melting of Type B CAIs: *Pressure*

- with melilite mantle: *Type B1*
- w/o melilite mantle: *Type B2*
- depletion of melt surface in Mg & Si due to higher evaporation rates compared to diffusion rates in melt
- Type B1: evaporation of CAI melt in a gas with $P_{H_2} > 10^{-5}$ bar
- Type B2: evaporation of CAI melt in a gas with $P_{H_2} < 10^{-5}$ bar *(Richter et al., 2002, GCA)*

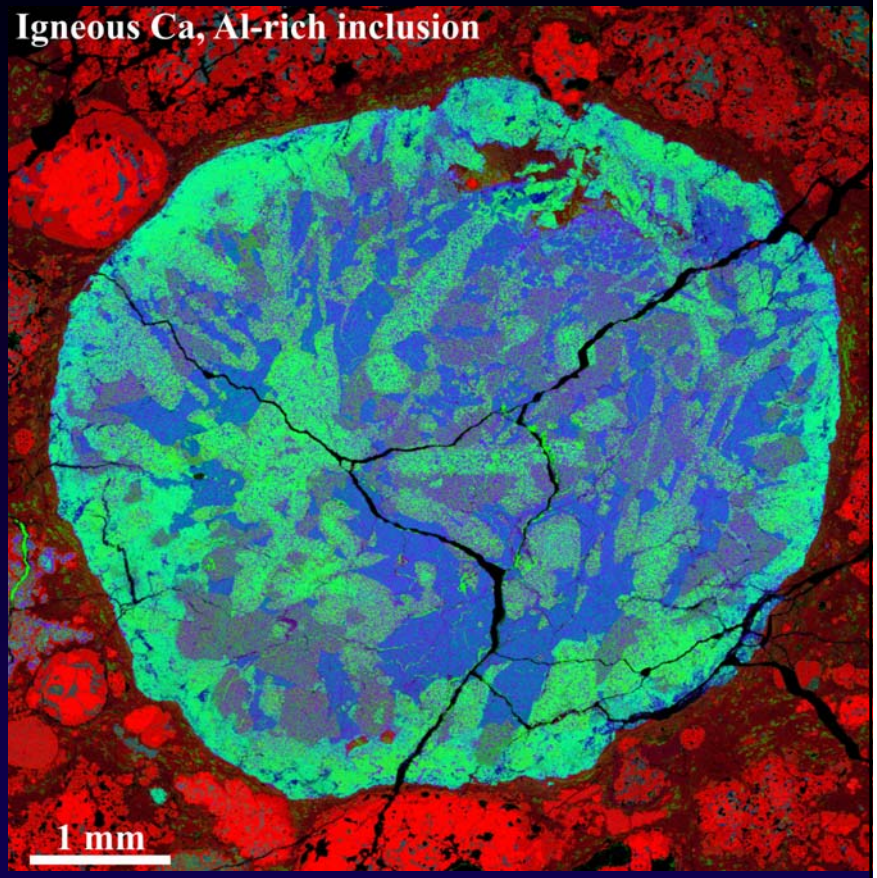

Constraints on melting of a CTA CAI

- Shahar & Young (2007) EPSL measured Si & Mg isotopic compositions in melilite of a CTA CAI by LA MC-ICPMS
- modeled chemical & isotopic effects of evaporation of a molten CAI; obtained a univariant relationship between P_{H2} & time during melting
  - ✓ CAI was molten for a cumulutive time of several hours to 15 days, depending on temperature & thermal history
  - ✓ CAI experienced subsolidis heating that produced diffusion limited isotope fractionation at its margin
- assuming equilibrium vapor pressure of gas component *i* (Mg, Si) for the CMAS melt is >> than ambient backgroung vapor pressure of *i* → number density of CAIs 10^{-3} to 2 m^{-3} (average linear separation of ~8 to 0.8 m)

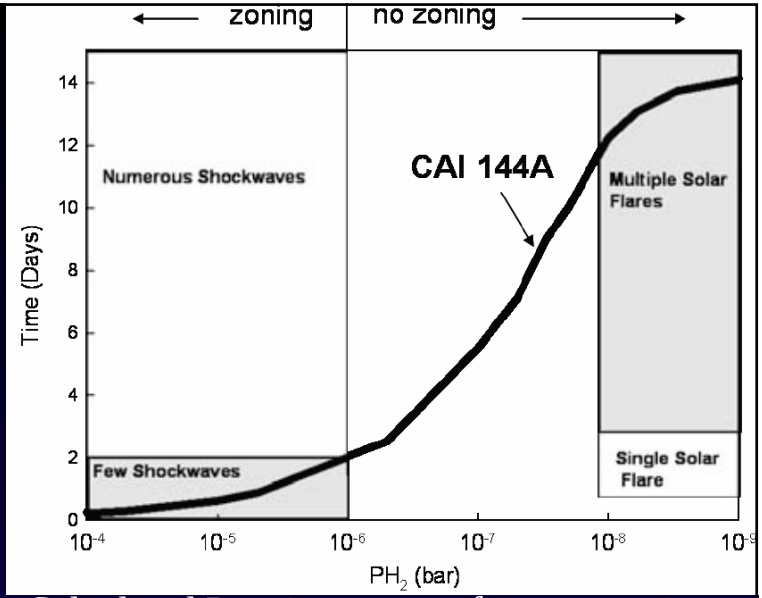

Calculated P_{H2}-time curves for evaporation of a molten CAI at 1773 K

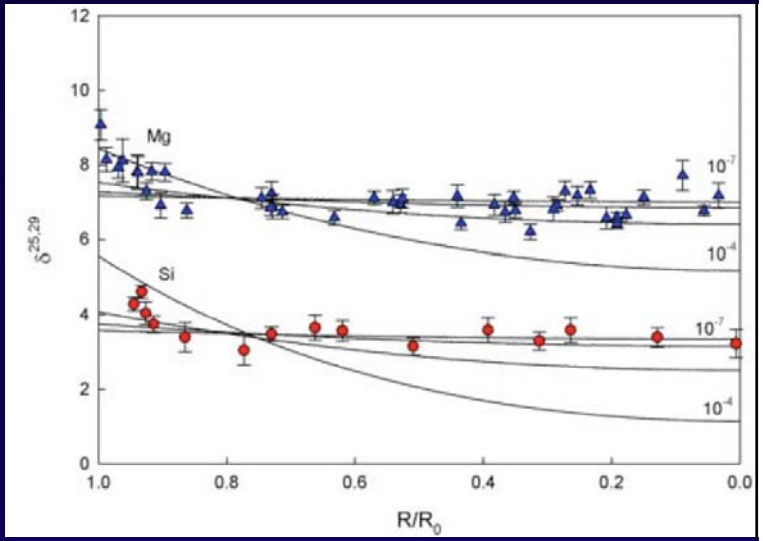

$\delta^{29}Si$ & $\delta^{25}Mg$ vs. distance from the center of CAI compared with calculated variations during evaporation at different P_{H2}. Sublimation of the solid CAI for 10 yr at T =1300 K and $P_{H2} = 10^{-7}$ bar.

Amoeboid olivine aggregates (AOAs)

- aggregates of CAIs & forsterite + Fe,Ni-metal condensates at ~1350-1450 K

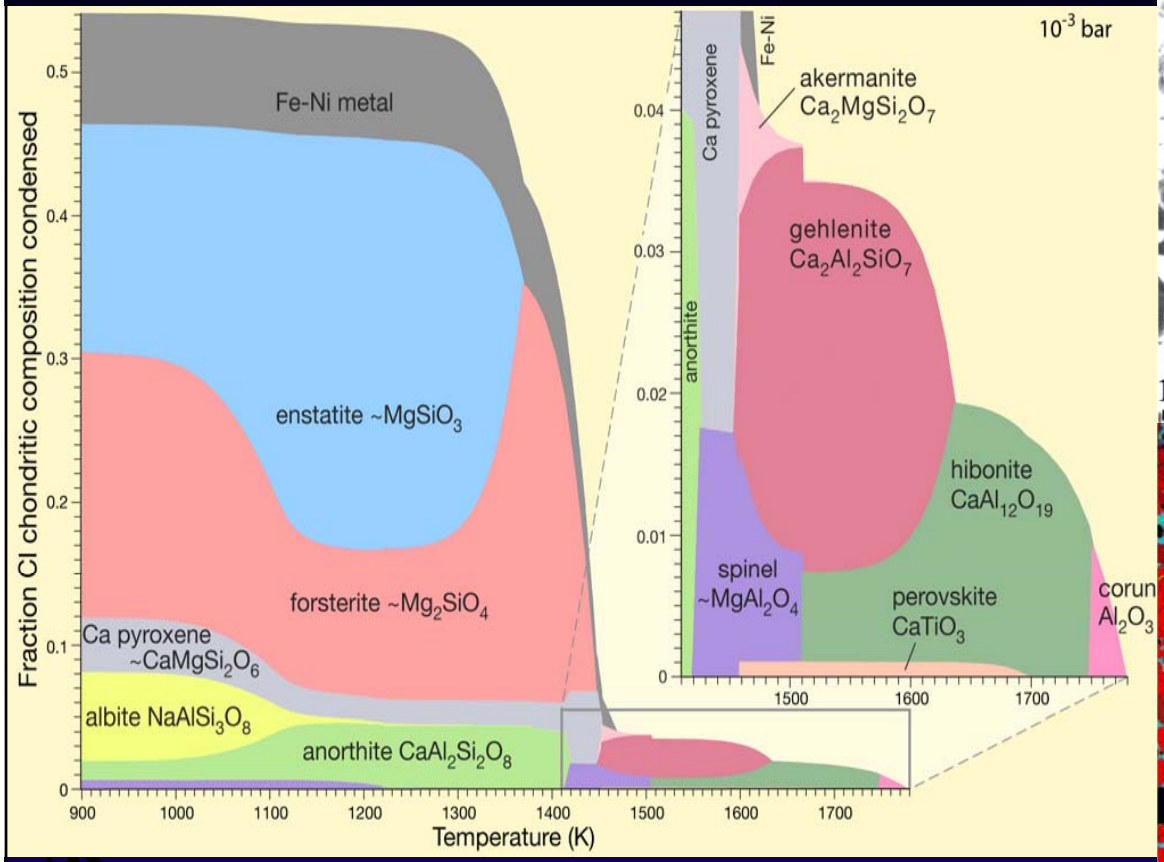

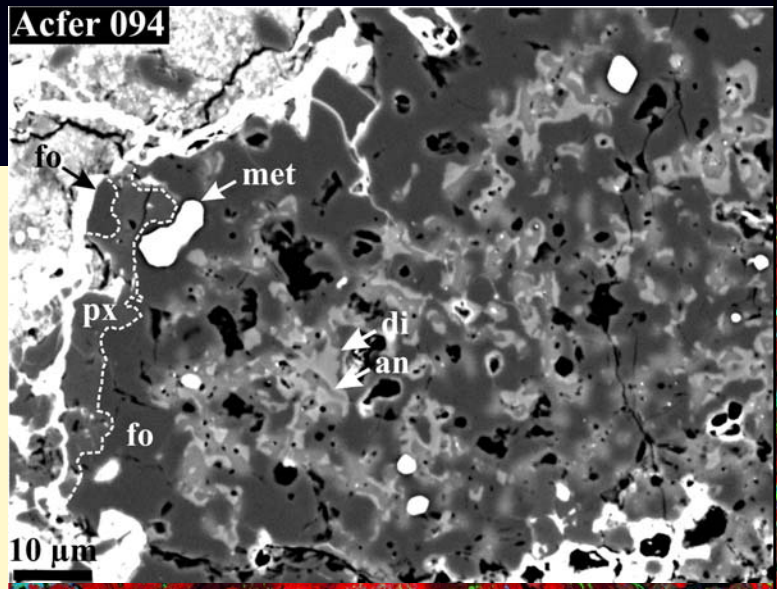

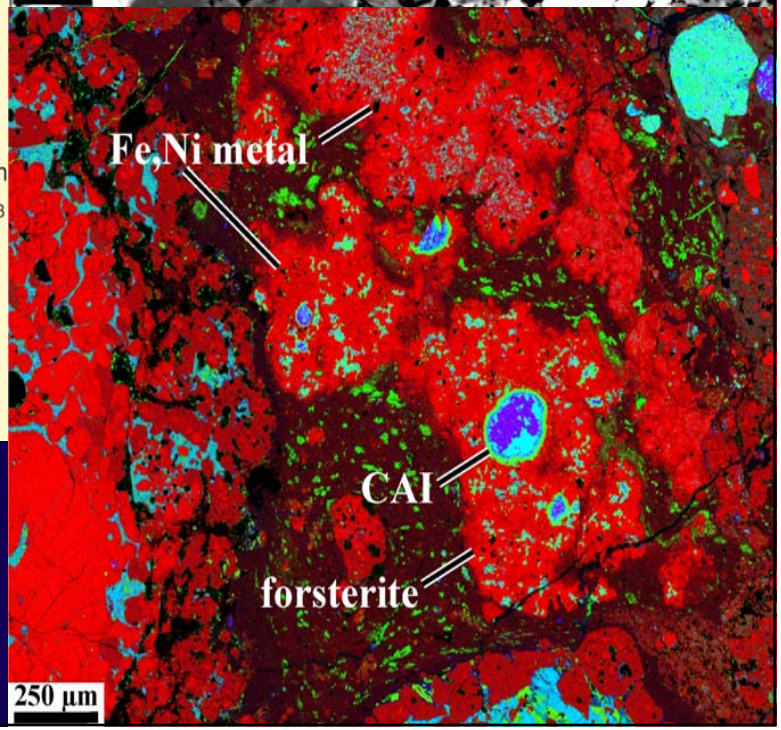

- CAIs & AOAs formed in the same nebular region (oxygen & Mg isotopes; next lecture)

Wark-Lovering & accretionary rims around CAIs

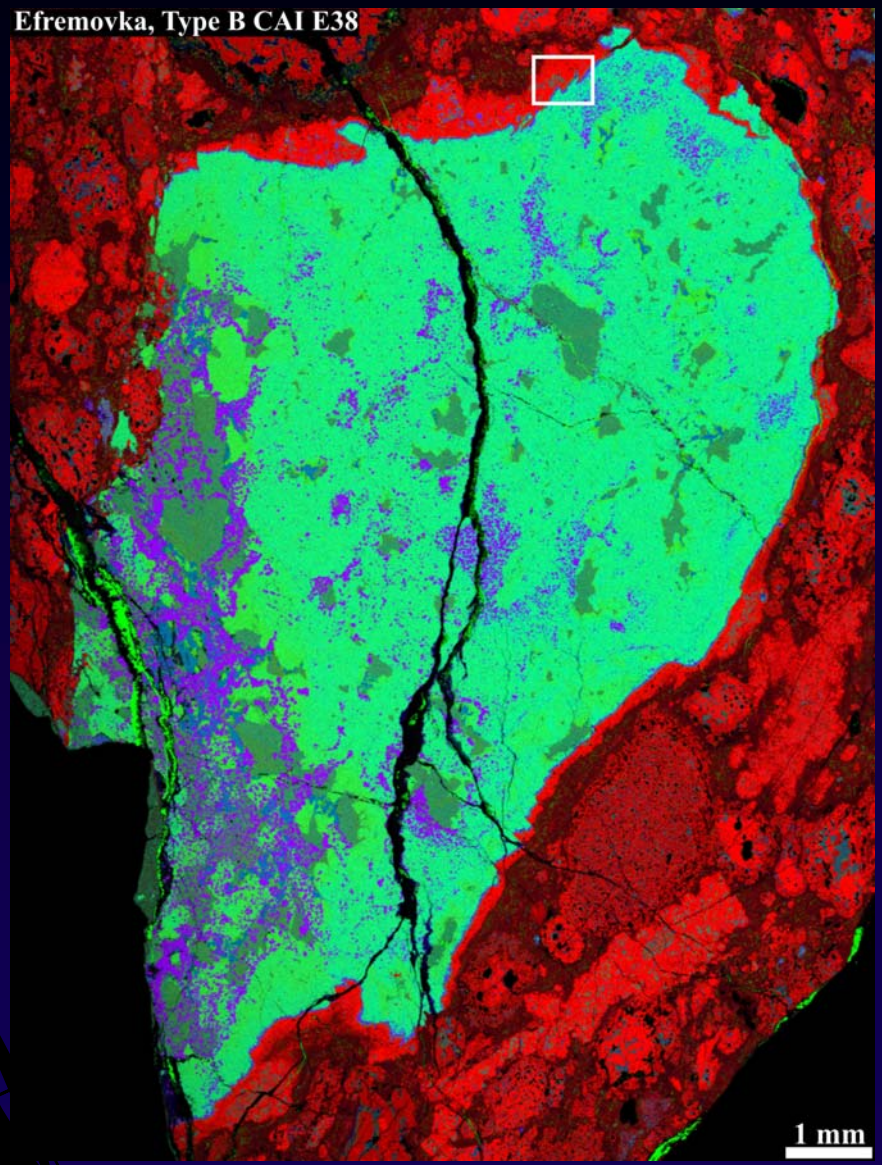

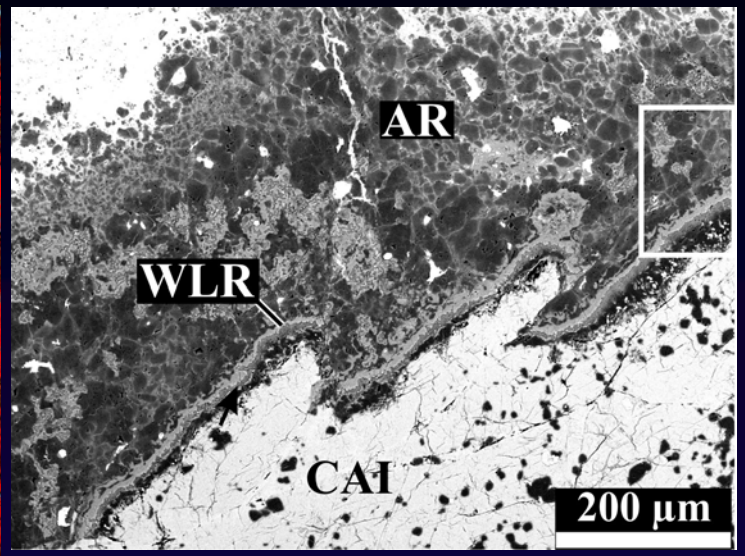

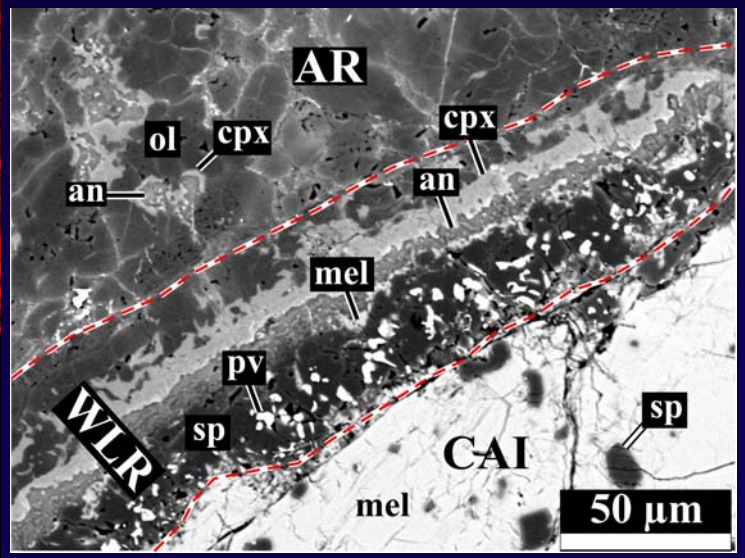

CAIs are the oldest solids formed in the Solar System

- ^{207}Pb-^{206}Pb ages of CV CAIs: 4567.11±0.16 Myr
- evidence for presence of short-lived radionuclides [^{10}Be, ^{26}Al, ^{41}Ca, ^{53}Mn, ^{60}Fe(?)]
- some preserved nuclear isotopic anomalies

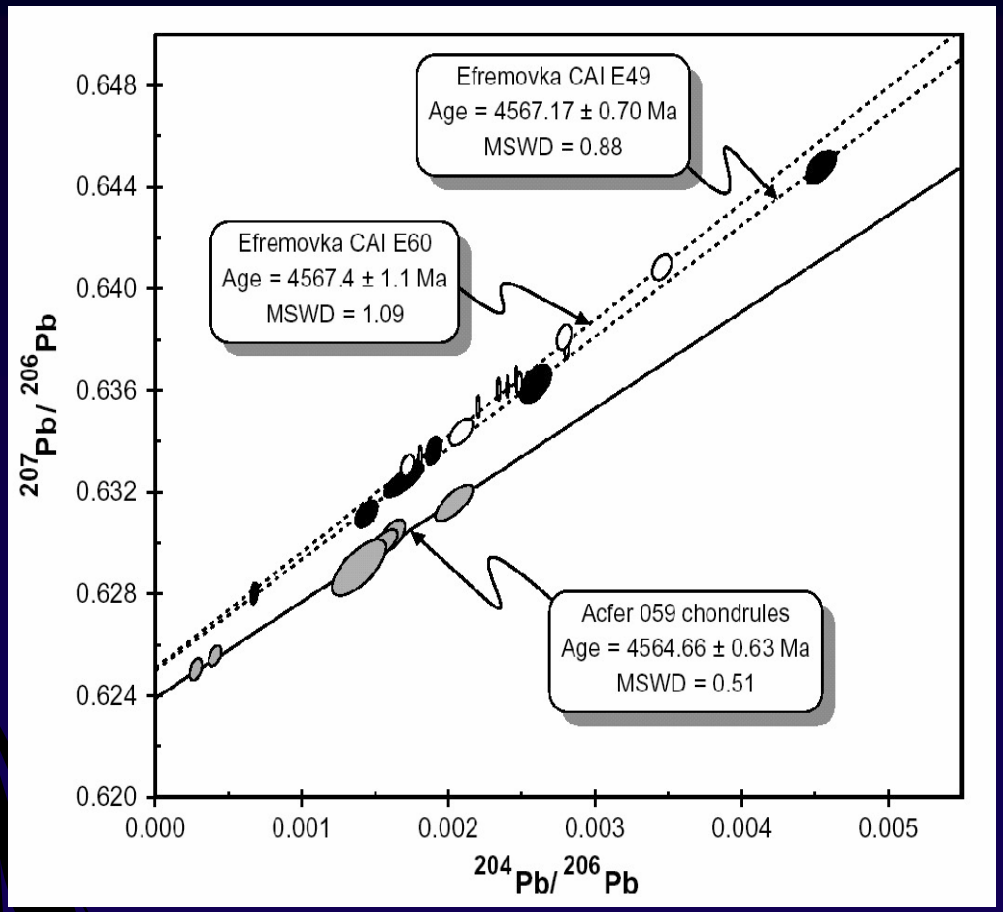

Amelin et al. (2002) Science

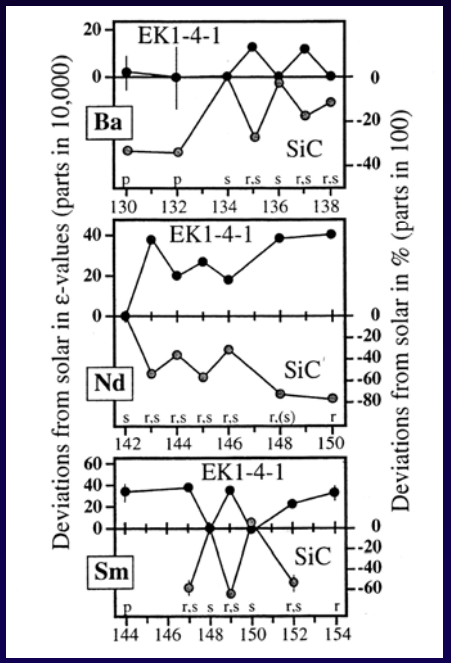

Begemann (1993)

CAIs & AOAs in primitive chondrites are ^{16}O-rich

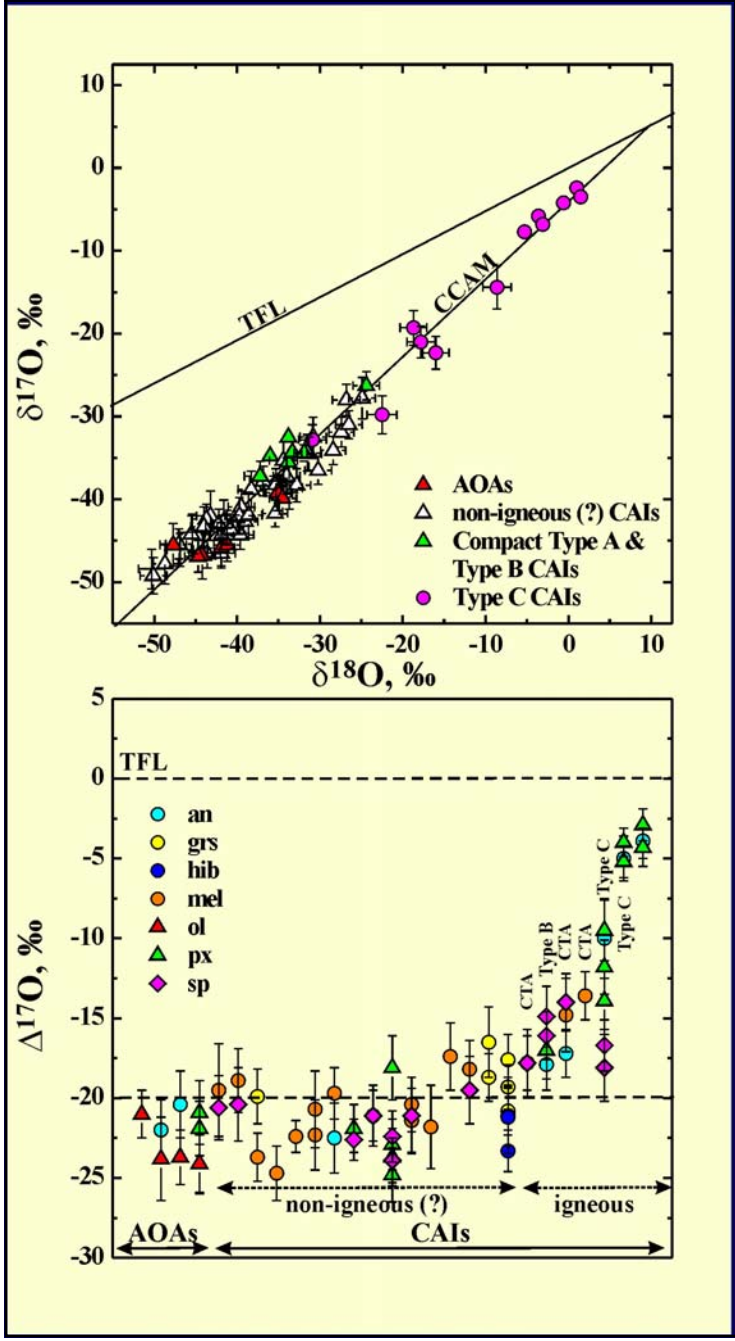

- CAIs & AOAs plot along slope-1 line
- AOAs & most CAIs in primitive (unmetamorphosed) chondrites are uniformly ^{16}O-rich
- some igneous CAIs are ^{16}O-depleted

- $\delta^{17}O = [(^{17}O/^{16}O)_{sample}/(^{17}O/^{16}O)_{SMOW} - 1] \times 1000$
- $\delta^{18}O = [(^{18}O/^{16}O)_{sample}/(^{18}O/^{16}O)_{SMOW} - 1] \times 1000$,

  where SMOW is Standard Mean Ocean Water
- $\Delta^{17}O = \delta^{17}O - 0.52 \times \delta^{18}O$

Constraints on the origin of CAIs & AOAs: Summary

- early, possibly within 10^5 years of Sun formation (next lecture)
- in nebular region(s) with ambient temperature >1350 K & ^{16}O-rich isotopic composition
- by evaporation-condensation processes
- some were subsequently melted (either by shock waves or by X-ray flares) at P_{tot} 10^{-4} – 10^{-9} bar & cooled at 1-100 K/hr
- number density of CAIs 10^{-3} to 2 m^{-3} (linear separation of ~8 to 0.8 m)
- under ~solar redox conditions (variations in dust/gas ratio up to 50 × solar may be required to explain chemistry of AOAs & WL-rims)
- subsequently were isolated from hot nebular region

Chondrules are less refractory than CAIs & AOAs

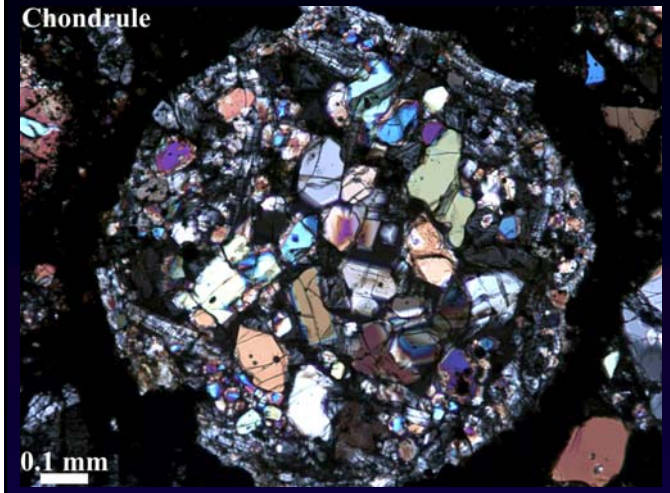

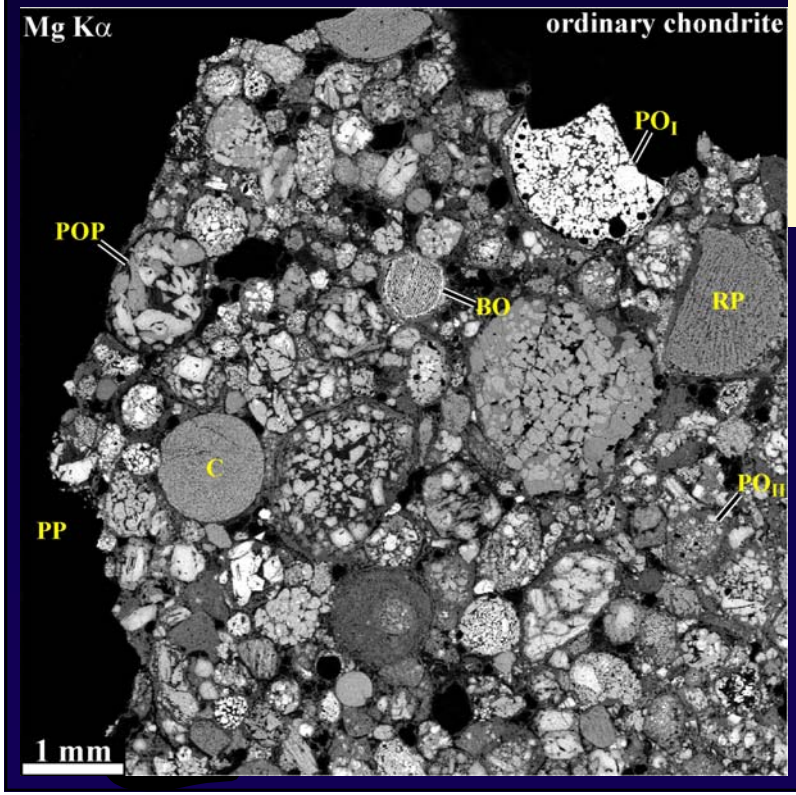

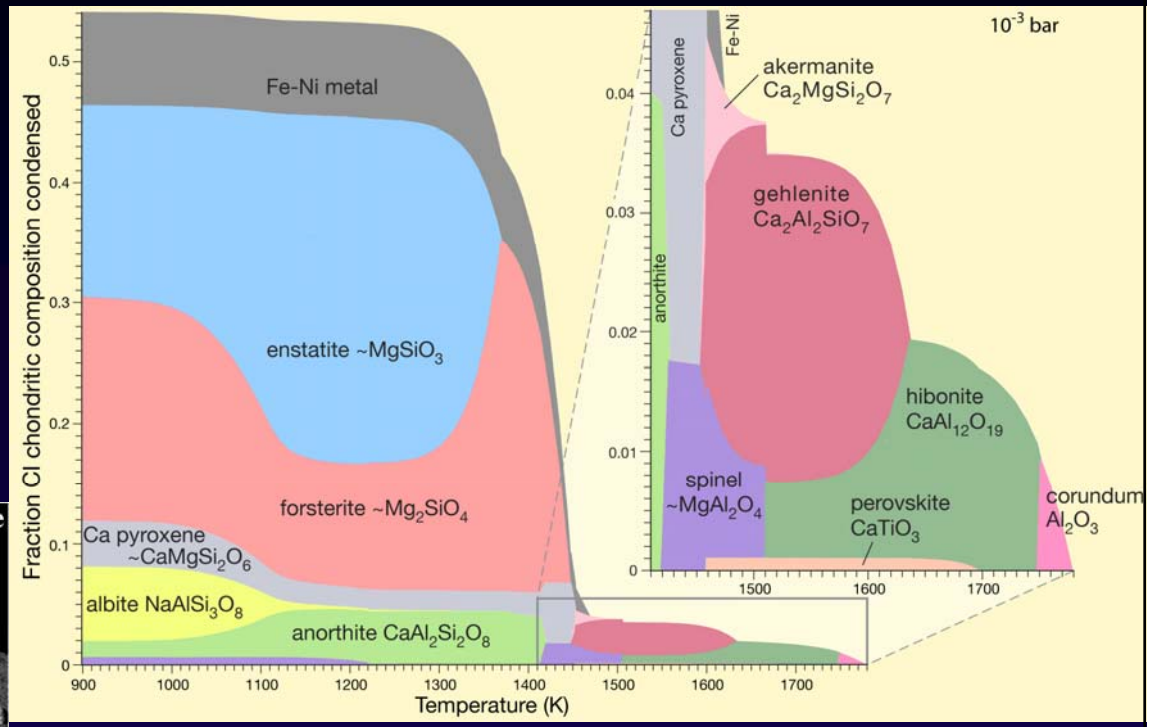

- igneous objects, ~0.01-10 mm in size, composed largely of Fe,Mg olivine & pyroxene, Fe,Ni-metal, & glassy or microcrystalline mesostasis

Diversity of chondrule textures, mineralogy & chemistry

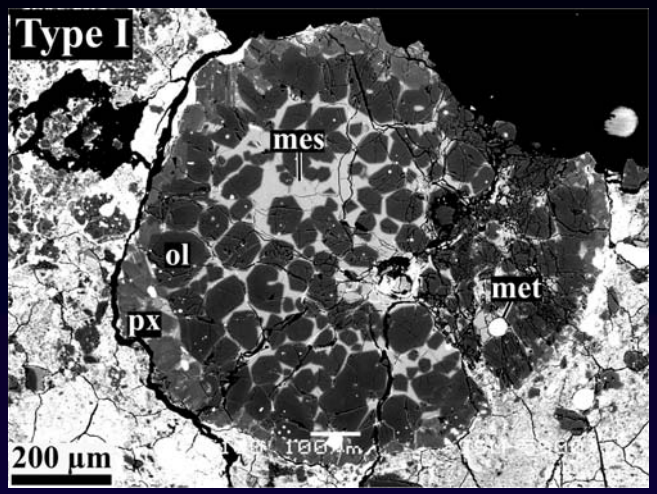

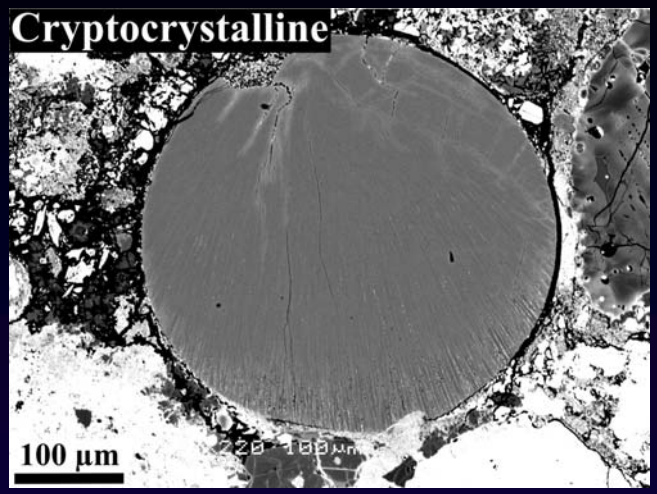

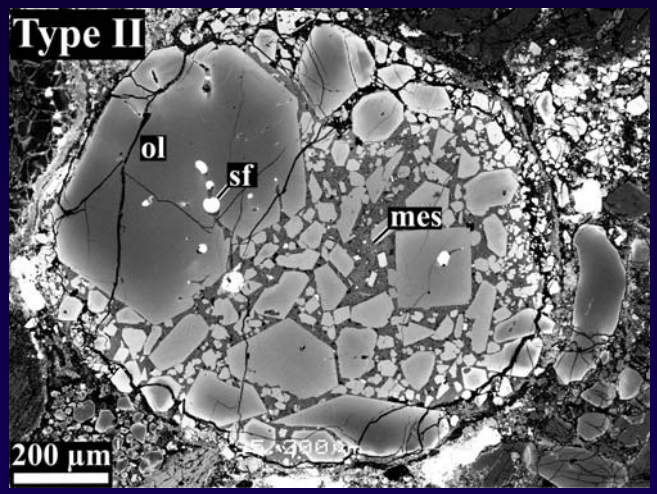

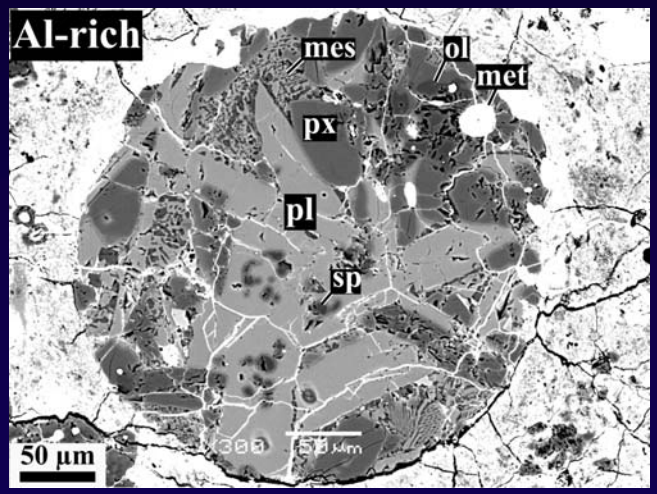

- most chondrules have porphyritic textures
- major chemical types: FeO-poor (Type I), FeO-rich (Type II) & Al-rich

Chondrules formed by repeatable heating events

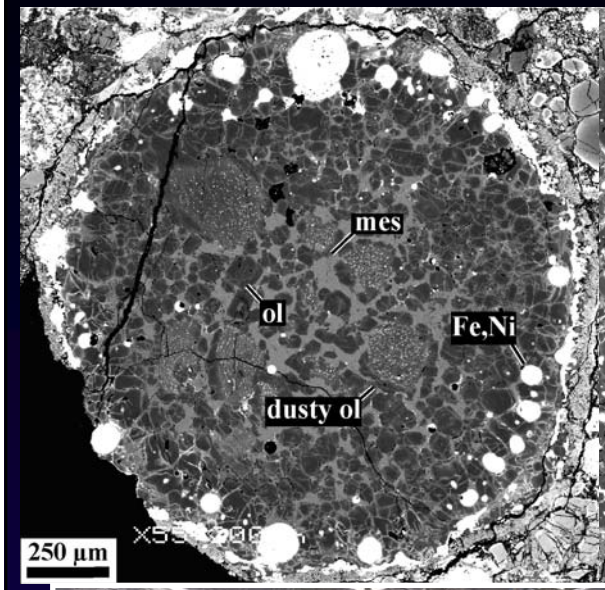

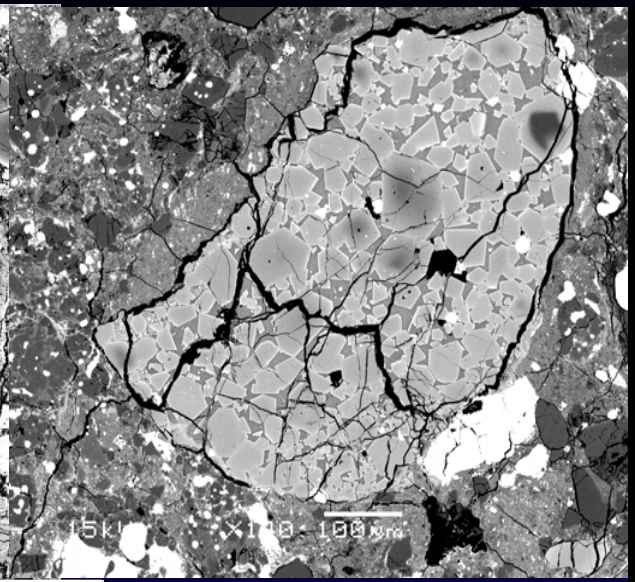

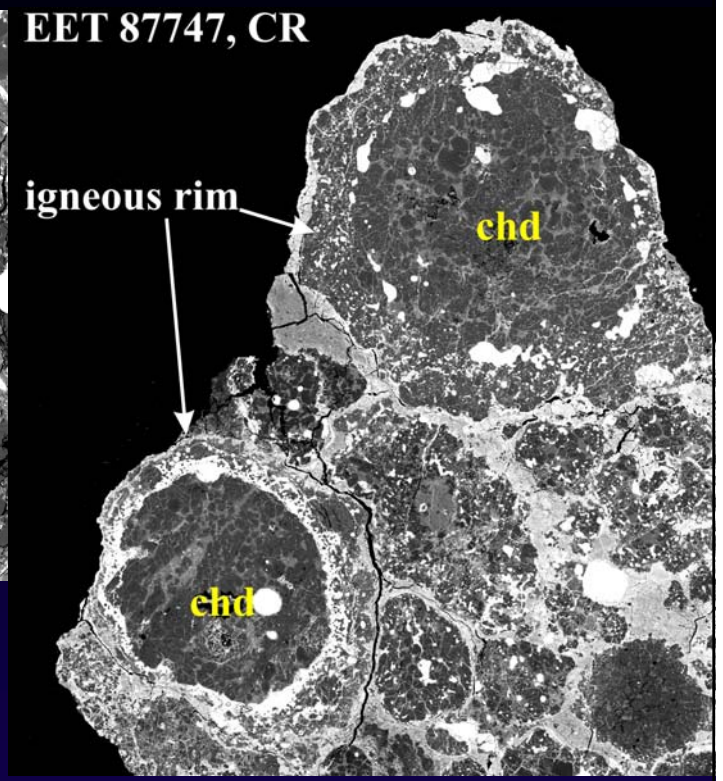

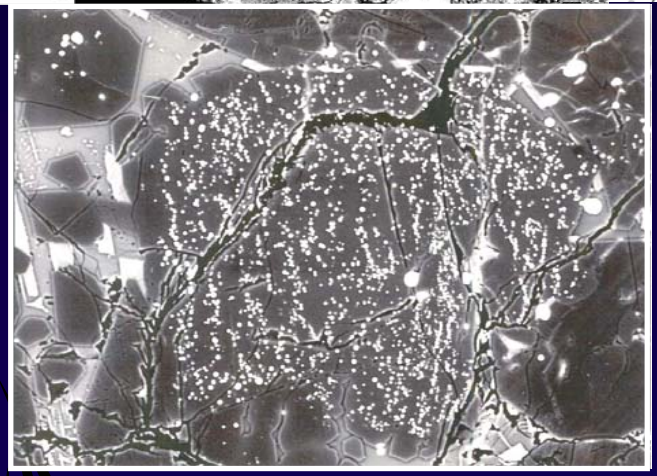

$Fe_2SiO_4 + C = 2Fe + SiO_{2(in\ melt)} + CO_2$

- relict grains & igneous rims suggest chondrule-forming events were repeatable

Precursor dustball hypothesis

- chondrules formed by melting of dustballs composed of fine-grained material (crystalline or amorphous) & a coarse-grained component
- fine-grained component was similar to matrix
- coarse-grained component consisted of fragments of earlier generations of chondrules & refractory inclusions

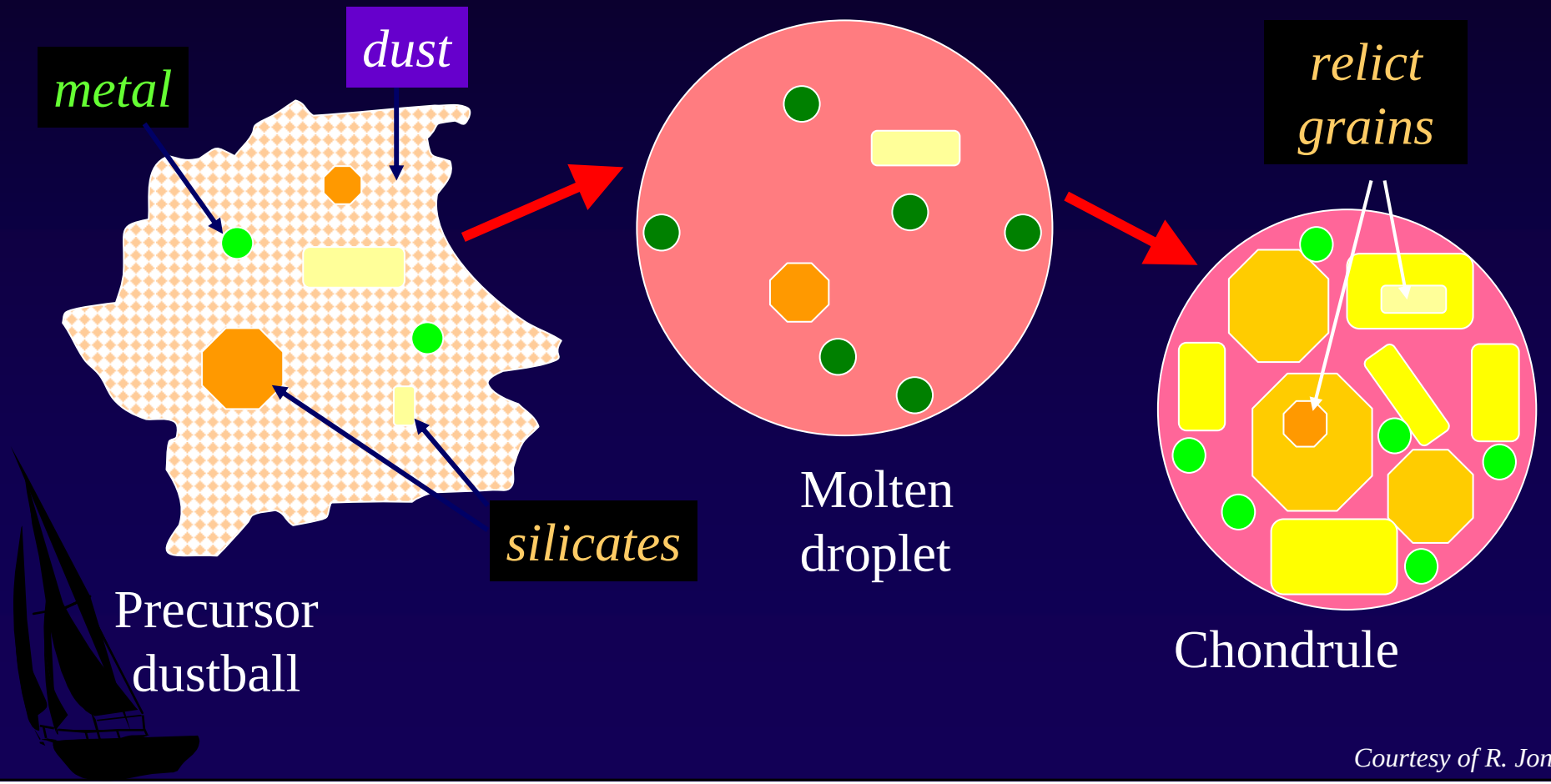

Courtesy of R. Jones

Experimental & observational constraints on melting of chondrules

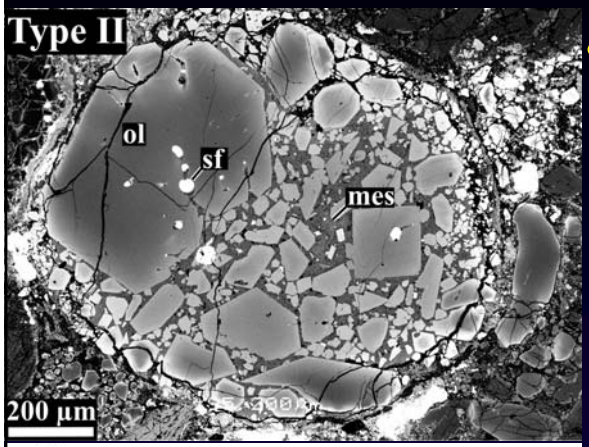

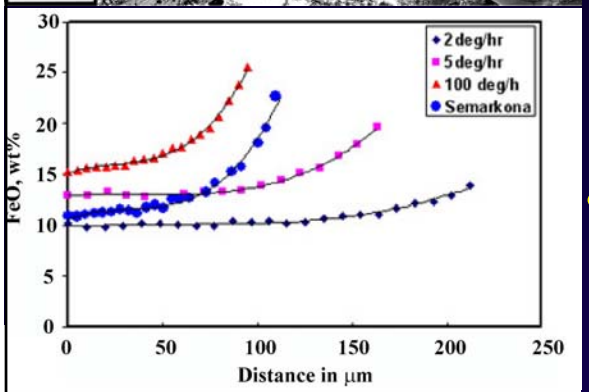

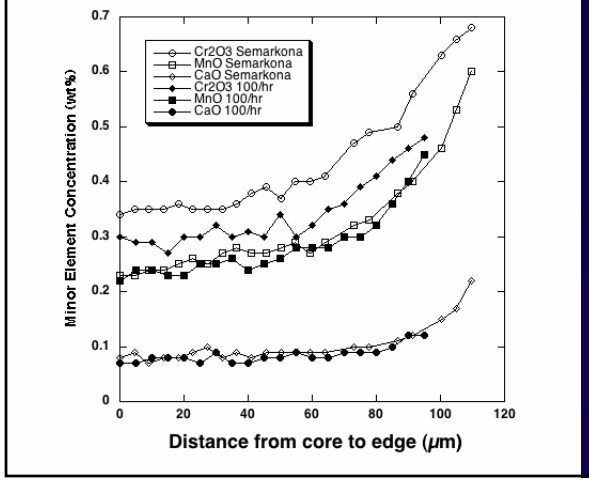

- chondrule textures, major & minor element zoning, high abundance of volatile elements
  - ✓ heating within minutes
  - ✓ peak heating temperature ~1650–1850 K
  - ✓ growth from a melt cooling at 100–1000 K/hr
  - ✓ evaporation of Na is suppressed under oxidizing conditions

- no evidence for mass-dependent isotope fractionation of K, Fe, Si & Mg (<1 ‰/amu)
  - ✓ isotopic fractionation could be *suppressed* at high $P_{total} = 10^{-3}$–10^{-4} bar & enhanced dust/gas ratio (~1000 × solar)
  - ✓ isotopic fractionation could be *erased* if vaporized gas back reacts with chondrule melt (number density of chondrules ~10 m^{-3})

Hewins et al. (2005) CPD

Experimental & observational constraints on melting of chondrules

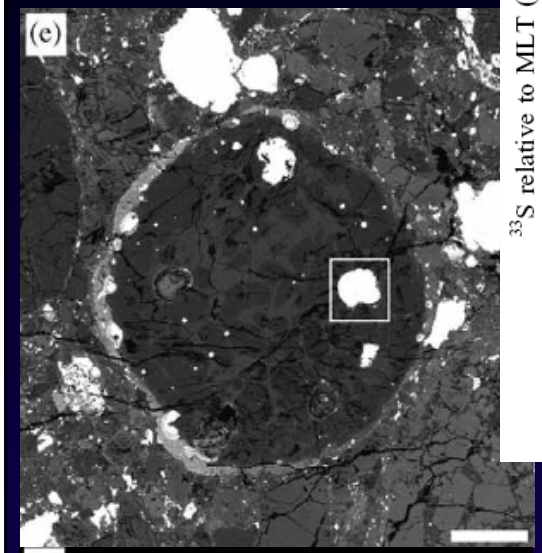

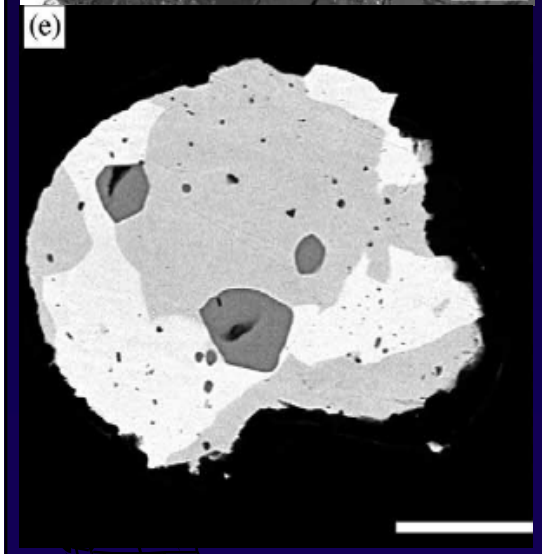

Tachibana & Huss (2005) GCA

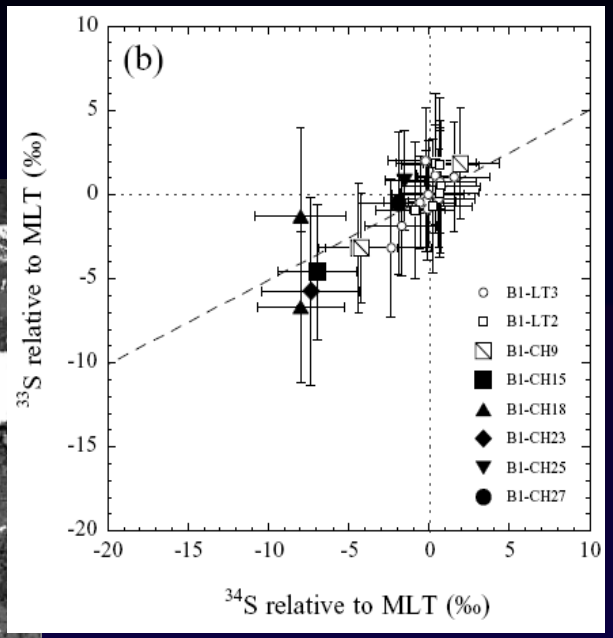

$$\delta^{34}S(‰) = \left(\frac{(^{34}S/^{32}S)_{meas}}{(^{34}S/^{32}S)_{MLT}} - 1 \right) \times 1000$$

$$\delta^{33}S(‰) = \left(\frac{(^{33}S/^{32}S)_{meas}}{(^{33}S/^{32}S)_{MLT}} - 1 \right) \times 1000$$

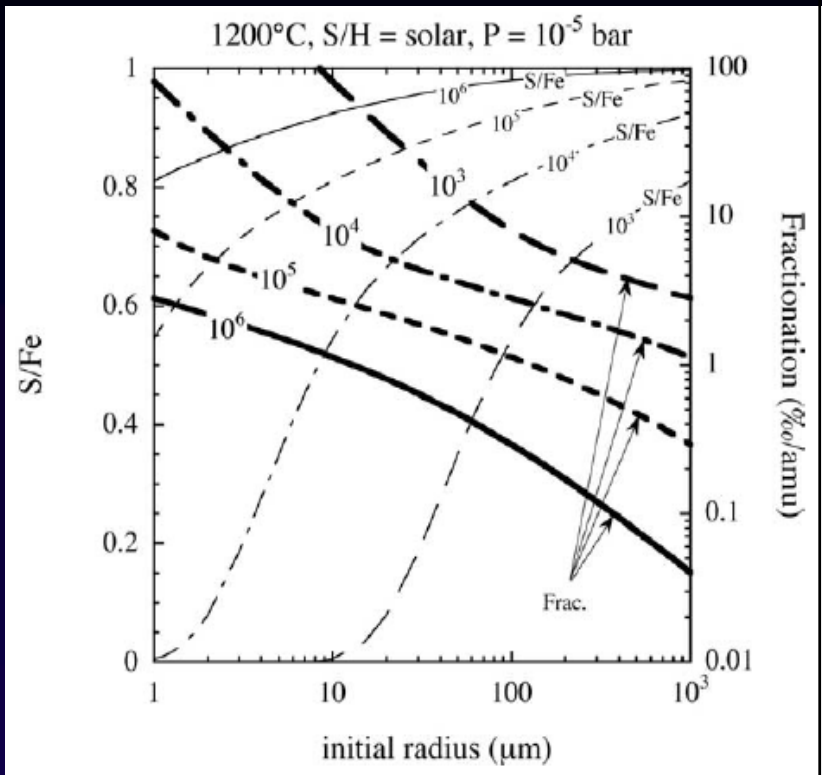

Fig. 7. The Fe/S elemental ratios (thinner lines) and the sulfur isotopic fractionations of the bulk condensed phase (thicker lines) heated with various heating rates up to 1200°C plotted against the initial grain size.

- high heating rate (>10^4-10^6 K/hr) is required to suppress S isotopic fractionation from Fe-S melt before silicates were melted extensively

Open-system behavior of chondrule melts

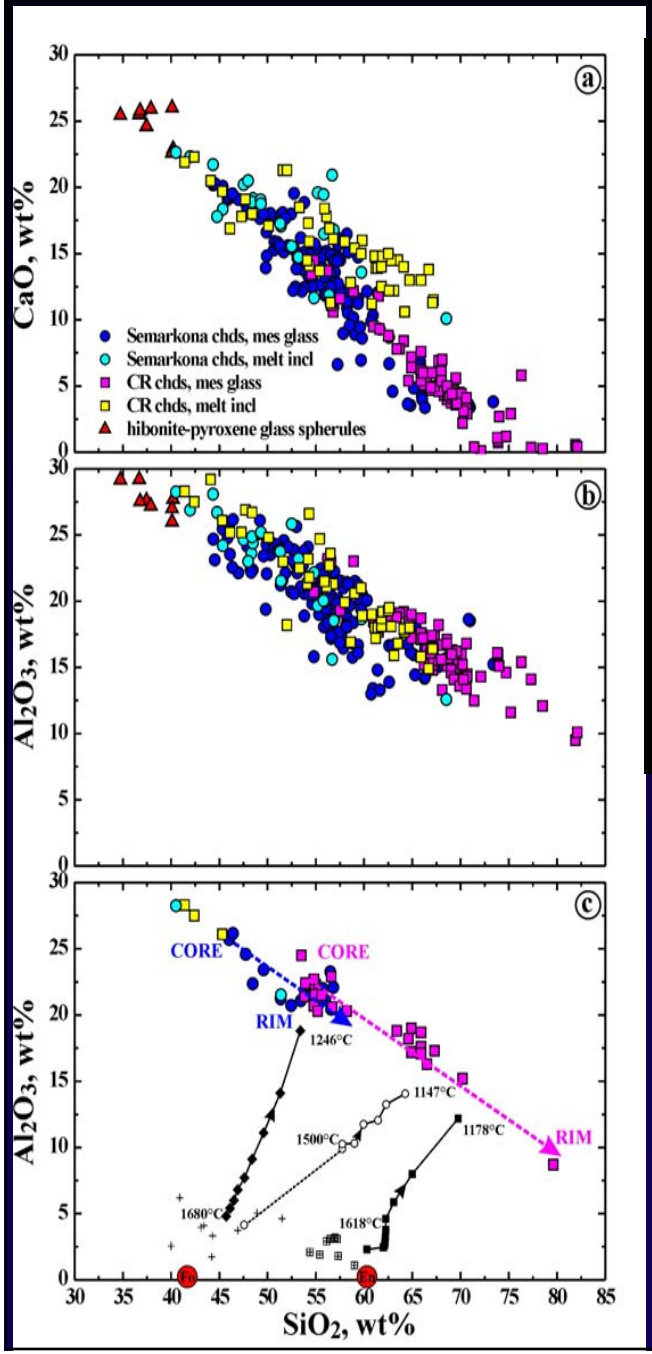

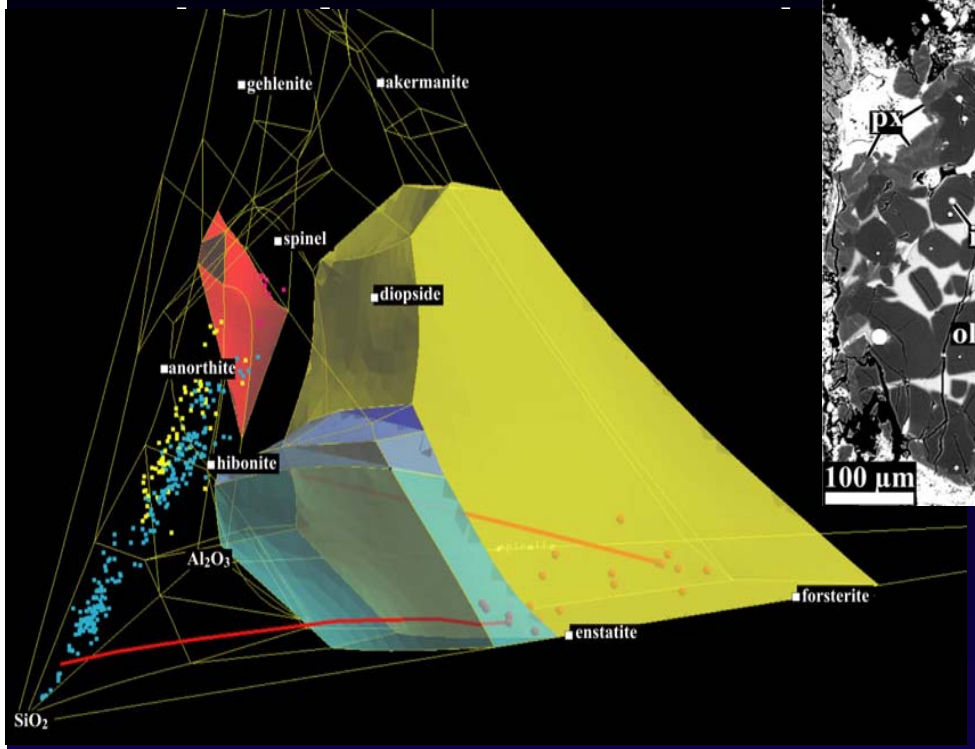

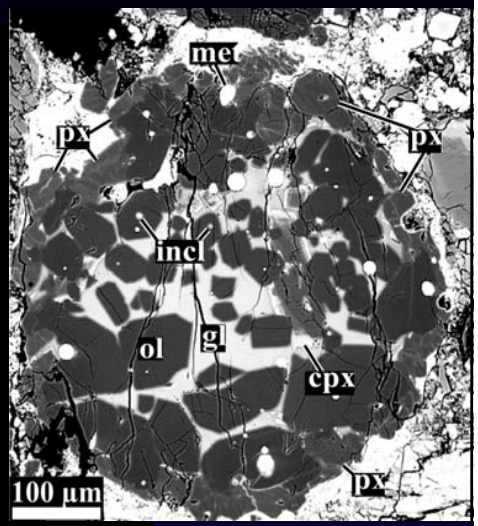

- radial min. & chem. zoning in Type I chondrules: $Mg_2SiO_4 \rightarrow Mg_2Si_2O_6 \rightarrow SiO_2$; increase of Si, Mn, Cr, Na, & K towards chondrule peripheries
- melt composition of Type I chds is not controlled by crystallization of olivine or pyroxene → Si & other elements condensed into chondrule melts

Libourel et al. (2006) EPSL

Presence of asteroidal material among chondrule precursors?

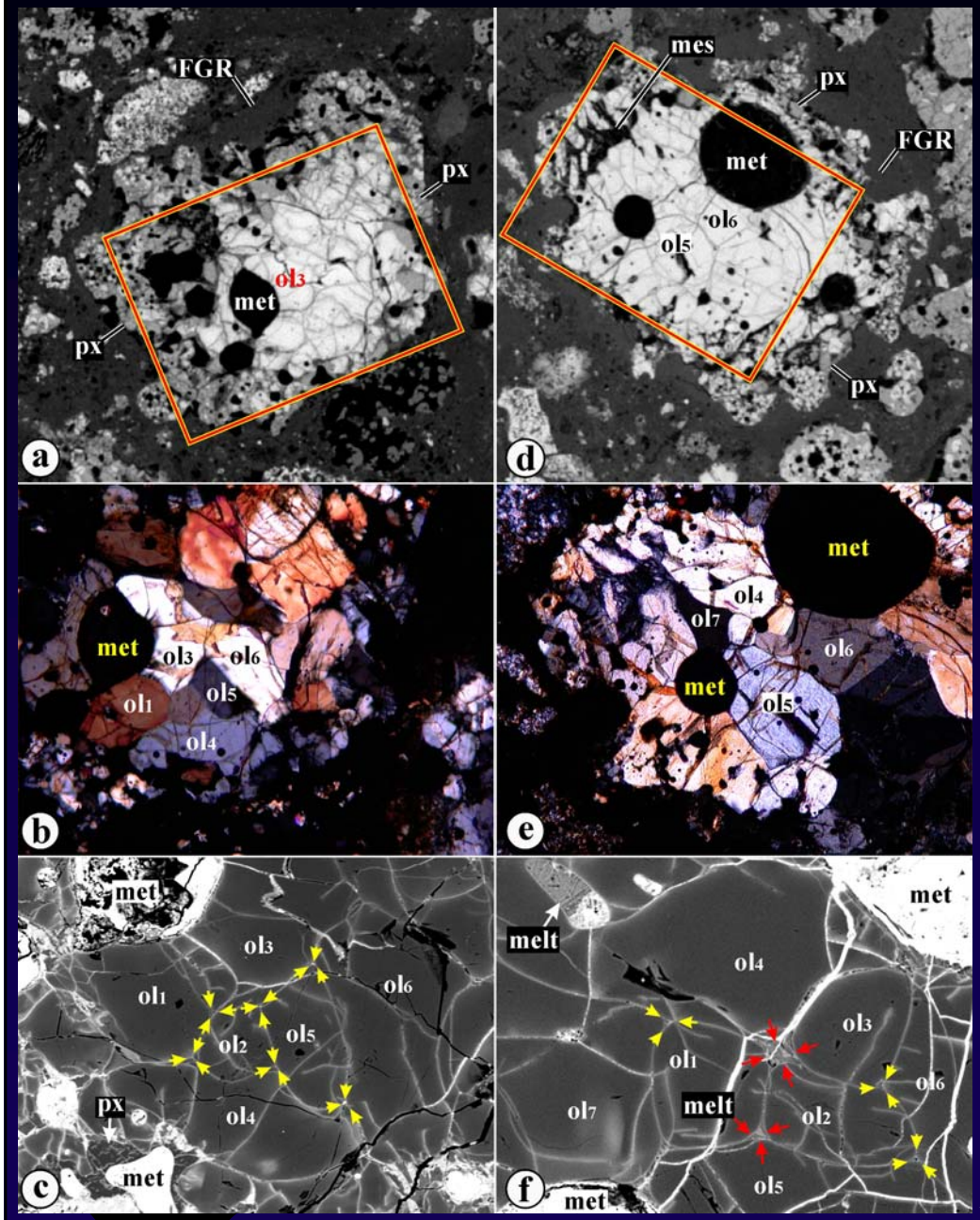

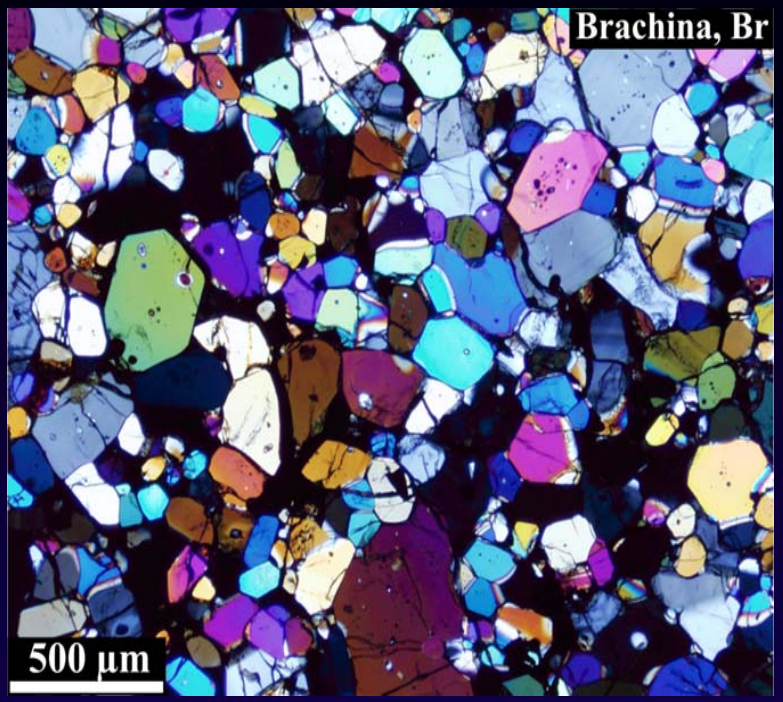

- some Type I chondrules contain relict lithic clasts of forsteritic olivine & ±Fe,Ni-metal with granoblastic textures requiring annealing at high temperature for several days (fragments of early planetesimals?)

Libourel & Krot (2006) EPSL

Chondrules are ^{16}O-depleted compared to CAIs & AOAs

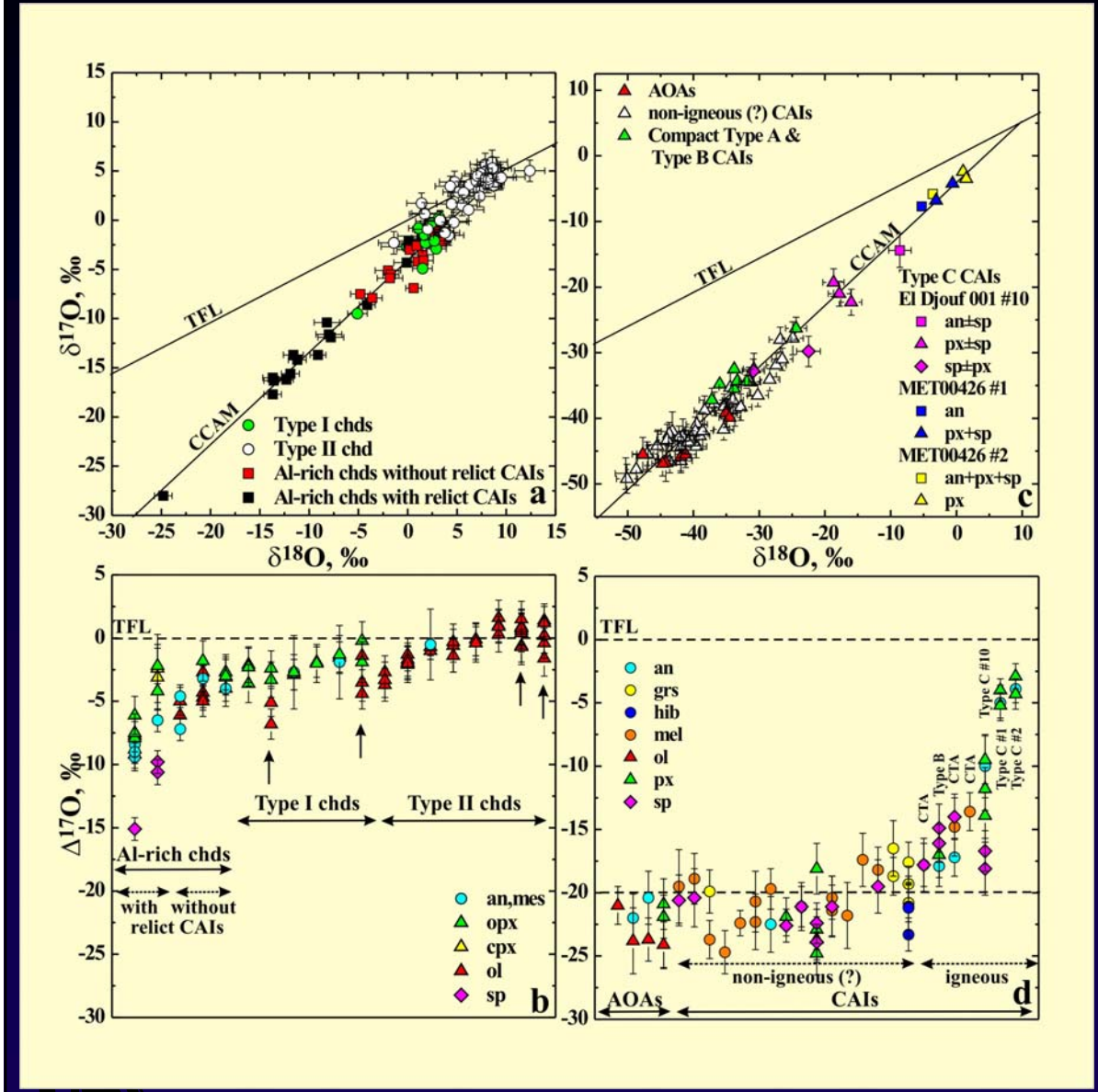

- ^{16}O-depleted compared to CAIs & AOAs
- some igneous CAIs are similarly ^{16}O-depleted (were remelted during chondrule melting)

Constraints on the origin of chondrules: Summary

- formed over several Myr (next lecture) by melting of solid precursors
- at lower ambient temperature (<600-1000 K) than CAIs (>1350 K)
- in a more ^{16}O-poor gaseous reservoir ($\Delta^{17}O > -5‰$ *vs.* $<-20‰$)
- under more oxidizing conditions than CAIs & AOAs
- under high P_{tot} ($>10^{-3}$ bar) & dust/gas ratio (up to 1000 × solar) or high number density of chondrules (10 m^{-3}) (linear separation of 10 cm^{-1})
- during multiple transient heating events of unknown nature (shock waves)
  - ✓ heating at 10^4-10^6 K/hr
  - ✓ peak heating temperature ~1650-1850 K
  - ✓ cooling rates 10-1000 K/hr